Gold Nanoparticle-Lipid Bilayer Interactions

By

Thomas Derrien

Department of Chemistry
McGill University
Montreal, Quebec

A thesis submitted to McGill University in partial fulfillment of the requirements of the degree of

Master of Science

October, 2009

For Mom and Dad.
Your never ending support and inspiration has made this possible.

ACKNOWLEDGEMENTS

Though the present thesis bears only my name, it is undeniably the work of countless persons. I am truly fortunate to have been in the presence of such committed and helpful individuals while completing this work.

First, I would like to thank my supervisor Prof. Bruce Lennox, whose guidance and mentorship, despite an incomprehensibly busy schedule, was always available when necessary. This project's course was not always visible but your quick insight ensured the proper steps were taken to redirect me down the correct experimental path.

The chemists in my group comprise a formidable team. The breadth of knowledge acquired from the members of the Lennox group, be it chemical or poker-related has been invaluable. Without Gopan's knowledge of lipid chemistry (giant vesicles are indeed useful!), I'm uncertain where I would have began with this project. Adil was my first teacher in the laboratory, I'm not sure how you tolerated such a sloppy chemist, but I thank you for it. I wouldn't be nearly as learned a nanoparticle chemist if it weren't for Paul's insistence on explaining seemingly minute mechanistic detail, additionally, your couch has proven a comfortable home from which to write this thesis. Aside from keeping me company in the lab Vishya and Gilles were always there to point out the obvious experimental details I had overlooked. Comedy seems to me to be the best form of stress relief in a graduate student's life, and Jon and Brendan could always be depended on for coffee breaks providing just that. Lastly, the group has seen its fair share of talented members come and go: Andreas made organic chemistry seem useful to an inorganic chemist; Marie's organization made stress-free group planning possible; Bill's unrelenting work-ethic never ceased to guilt me into working, Simona could always be relied on to answer my seemingly silly questions, despite being thousand of miles away, and finally Marco's vacationing and photography skills made the summers that much better. Although not a chemist, Sandra is certainly a much needed group member!- Thank you all.

A special thanks goes out to Dr. David Liu for fast and reliable TEM imaging and to Dr. An Beum-soo for being such a patient collaborator.

Finally I would like to thank my family. My younger brother Gauthier, aside from never answering his phone was always available for good company, food and/or beverage. My older brother Nicolas did a great job at feigning interest in my work, thanks for listening, or at least pretending to. Lastly, thank you Mom and Dad, for your unending love and support. Not a day passes without my recognizing how lucky I am to have you.

ABSTRACT

The interactions of ligand-capped gold nanoparticles with lipid bilayers are investigated. The properties determining the mechanism of nanoparticle interaction using synthetic membrane models are explored. First, a specific interaction, incorporation of nanoparticles into the bilayers, is examined using novel imaging and nanoparticle synthesis techniques. Mixed ligand capped gold nanoparticles are synthesized with assorted ligand arrangements in order to relate ligand composition and structure to interaction mechanism using a dye leakage assay. Finally, *in vivo* experiments are conducted using peptide labeled fluorescent gold nanoparticles in live HeLa cells. It was found that gold nanoparticles are capable of crossing lipid bilayers, implying energy-independent cellular uptake mechanisms may occur. It is concluded that the structure and composition of the protecting ligands are critical in determining the magnitude of bilayer disruption.

ABRÉGÉ

L’interaction des nanoparticules d'or avec les bicouches lipidiques est présentée dans ce mémoire. Les facteurs influençant cette interaction ont été explorés en utilisant des bicouches lipidiques synthétiques. L’interaction due à l’incorporation des nanoparticules au sein des bicouches a été étudiée par des techniques d'imagerie. Un test de fuite de fluorophore a été employé afin de déterminer l’influence de la composition et de la structure des ligands protégeant les nanoparticules sur leur incorporation dans les bicouches de lipides. Pour cela, nous avons développer une synthèse de nanoparticules protégées par deux types de ligands. Des expériences *in vivo* ont été réalises avec des nanoparticules d'or fonctionnalisées avec des peptides ainsi que des fluorophores, mis en contact avec des cellules vivantes de type HeLa. Nous avons constaté que les nanoparticules d'or sont capables de franchir les bicouches lipidiques en utilisant des mécanismes indépendants d'énergie. Nous concluons que la structure et la composition des ligands protégeant les nanoparticules ont une grande influence sur la perturbation qu’elles induisent dans la structure des bicouches lipidiques.

Table of Contents

CHAPTER 1

General Introduction

The recent convergence of nanotechnology and medicine has brought forth both a number of promises and questions. From new imaging techniques[1] to novel cancer treatments[2], nanomedicine has the potential to overcome some limitations inherent to "macro" medicine. In particular, the use of nanoparticles for biomedical applications *in vivo* has been extensively explored. Nanoparticle formulations have even made it to clinical trials. Aurimmune®[3], a gold-nanoparticle based cancer therapy, is currently undergoing Phase I clinical trials. Although the effectiveness of nanoparticle-based medicine is yet to be established, much remains to be elucidated about the basic biology related to the interactions of these systems with the living cell. In order to properly understand cellular uptake, distribution, and above all, toxicology, nanoparticle-membrane interactions must be fully understood.

Several methodologies have been developed to study the possible interactions of nanoparticles with lipid membranes. Theoretical calculations and artificial membrane mimics are essential in gaining a preliminary understanding of the interactions in the absence of cellular functions. After thorough study of these techniques, it is possible to investigate the action of nanoparticle systems in living cells, either *in vitro* or *in vivo*.

1.1 LIPID BILAYERS AND CELL MEMBRANES

In order to elucidate the mechanisms of nanoparticle interactions with cell membranes one must first gain an understanding of the structure and dynamics of the

lipid membrane. This section is intended to provide the reader with a brief introduction to the concepts of lipid membrane structure and function.

Questions about cell structure arose in the 17th century with the advent of the microscope, when cells were viewed for the first time. However, it wasn't until the arrival of the Langmuir-Blodgett trough, three centuries later, that the 'plasma' membrane structure would be correctly deduced. Using the same methods employed by Langmuir to measure the areas of films of red blood cell lipids, two Dutch scientists, Gorter (a physician), and Grendel (a chemist), discovered that the area the lipids occupied was twice that of the area of the red blood cells. This led to the conclusion that the membrane is, in fact, two lipid molecules thick, generating the concept of the bilayer lipid membrane[4].

Most central to the properties of lipid membranes is the detailed structure of the bilayer. The charged, hydrophilic, polar head groups face the aqueous solutions on either side of the membrane, while the hydrocarbon, hydrophobic tails, self assemble to face one another (Figure 1.1). This geometry accounts for the apparent solubility of the water-insoluble lipids ($<10^{-9}$ M solubility) and the remarkable impermeability of the membrane to most ions and water-soluble reagents' permeability properties. The oily, or lipophilic, core greatly reduces the permeability of ionic and polar inorganic species, and only small solutes such as chloroform and ethanol will readily permeate a lipid bilayer membrane. In the cell, the lipophilic core can be generated by varying the composition of the lipids, where the gradient across the bilayer can be adjusted by introducing charged headgroups. This is achieved by including negatively charged lipid headgroups such as phosphatidylserine and phosphatidylinositol. The gradient may be even further

manipulated by shifting the distribution of these charged lipids to the outer and inner layer.

There are many factors that will govern the permeability properties of the membrane. For instance, transport across the membrane may be enhanced in the cell by including transport or surface proteins. The positioning of these proteins within the lipid membrane was first conceptualized by Singer and Nicholson in 1972[5], in the form of their now classic 'fluid mosaic' (Figure 1.1[6]) model.

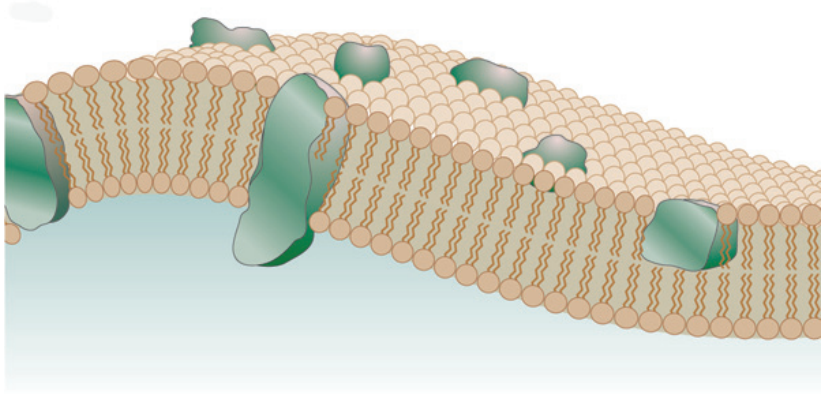

Figure 1.1: Fluid mosaic model of cell membrane

As previously alluded to, a nanoparticle crossing the cell membrane is not limited to direct interaction between the incoming particle and the lipids in the cell membrane. Particle uptake may take place via one of the many mechanisms specifically designed for this purpose. In order to fully understand the mechanisms through which nanoparticles interact with a cell, a complete understanding of both nanoparticle-lipid membrane interactions and *in vivo* nanoparticle-cell interactions must be developed.

1.2 LIPID MEMBRANE NANOPARTICLE INTERACTIONS

Taking into account the amphiphilic nature of the components of the cell membrane, three types of interactions of nanoparticles with the membrane can be envisaged (Figure 1.2). The first type of interaction (A) is electrostatic, in which the nanoparticle is bound to the surface of the membrane by simple electrostatic forces. The second type of interaction (B), involves a hydrophobic particle embedded into the core of the membrane. This is dominated by van der Waals interactions and the hydrophobic effect. Finally, (C) involves a complex combination of (A) and (B), where a nanoparticle partitions into the bilayers but is released to the other side.

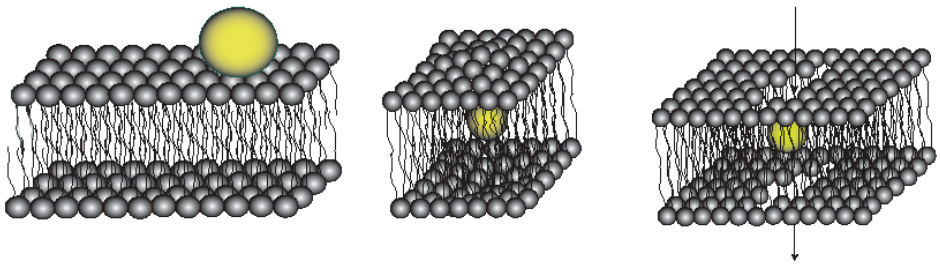

(A) **(B)** **(C)**

Figure 1.2: Possible interactions of nanoparticles with lipid membranes

The latter examples have been observed both experimentally and theoretically in model lipid systems. One notable example of the first type of interaction, adsorption to a liposome, has been observed with polystyrene nanoparticles[7]. These experiments illustrate the importance of the electrostatic interaction between the polar phospholipid headgroups, the zwitterionic phosphatidylcholine group, and the ligands coating the nanoparticle. Because of the polar nature of the headgroup, only hydrophilic particles will readily absorb onto the surface of the membrane. The driving force for this interaction is

dominated by enthalpic interactions derived from electrostatic and/or dipole-dipole interactions. For the neutral hydrophilic particle case the interaction is dominated by dipole-dipole interactions, while for a charged particle charge-dipole interactions dominate. The latter are stronger, and operate over larger distances. For this reason charged particles are more often employed for surface applications. Moreover, it has been suggested that the entropy gained by displacing water molecules by adsorbing nanoparticles may also favor adsorption[7].

Zhang and Granick[7] have exploited the nanoparticle-lipid bilayer phenomenon for use in stabilizing liposomes. Liposomes are spherical phospholipid bilayer assemblies that can serve as versatile models of cell membranes. Shaking or sonication of a dispersion of phospholipids(s) in water will produce these spherically symmetric bilayer assemblies whose interior volume is water. Multilamellar assemblies are generally termed liposomes whereas single lamellar assemblies are generally termed vesicles. The latter are formed with high energy input into a liposome solution, usually in the form of probe sonication. Alternative methods including extrusion of a liposome solution through well defined membrane holes (0.05-0.5 μm) also produce vesicles, often termed small unilamellar vesicles (SUVs). They have been frequently used as drug delivery systems. Their use is however often limited by their stability, as solutions of liposomes tend to flocculate after several days. Zhang and Granick showed that when nanoparticles adsorbed onto their surface, the liposome stability significantly increases. Solutions of up to 50% volume fraction were investigated, while untreated, zwitterionic liposomes were unstable above a 2% volume fraction. The stabilization scheme used in this case is straightforward, simply adding 20 nm charged latex nanoparticles (latex beads

functionalized with positively or negatively charged ligands) to an aqueous solution of liposomes promotes adsorption onto the surface. This method of stabilization, known as nanoparticle "haloing", was originally introduced by Tohver et al[8]. The stability is achieved by creating electrostatic repulsion between approaching nanoparticle halos. Anionic particles are thought to bind more strongly to the surface, as the charge is opposite to the outermost portion of the zwitterionic lipid headgroup (Figure 1.3).

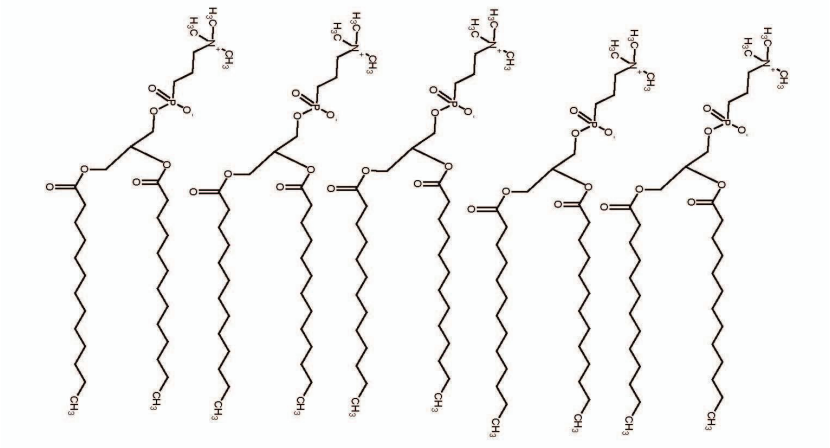

Figure 1.3: Arrangement of lipids in a phosphatidylcholine bilayer. Notice that the positive charge of the choline nitrogen is located on the outer surface (top).

Interestingly, this means that anionic particles will stabilize the zwitterionic liposomes less effectively, as strongly adsorbing particles are likely to bridge two liposomes[9]. Liposomal adsorption using gold nanoparticles has also been explored in a similar manner[10]. Urban *et. al.* mixed phosphatidylcholine liposomes with gold nanoparticles possessing a positively charged, cetyltrimethylammonium bromide (CTAB) ligand shell. The liposomes could then bind to the nanoparticles to form a gold nanoparticle-liposome conjugate. In contrast to the stabilization scheme of Zhang and Granick[7], the system in this case could be used to control the phase behavior of individual lipids on the nanoscale. Such behavior parallels that suggested by several theoretical studies carried

out. For example, Ginzburg *et. al.*[11] as well as Noguchi *et. al.*[12] have both separately noted similar interactions in the modeling of liposomes in contact with charged nanoparticles.

The second possible type of nanoparticle interaction with a lipid membrane is an incorporative one (Figure 1.2B). Incorporation of nanoparticles into the bilayer of lipid membranes has been extensively studied.[13-15] The embedding of nanoparticles into lipid bilayers has only been achieved thus far using artificial constructs such as liposomes. The primary interest in this type of structure is for use in drug delivery, particularly for controlled release purposes, and imaging, as nanoparticles can trigger the release of liposomal contents when exposed to UV radiation[16].

The long alkyl chains that make up the interior of the bilayer render this region highly hydrophobic. Consequently, only uncharged, non-polar particles are expected to remain in this region. Simulations conducted by Ginzburg and Balijepalli[11], concluded that uncharged particles reside in the bilayer, while charged particles induce defects in the bilayer. The lowest energy confirmations determined in this work anticipate that embedded nanoparticles would cause a protrusion on only one side of the bilayer. Such an arrangement, although difficult to prove experimentally is interesting, as it means that lipid tail-nanoparticle interactions vary on the surface of the particle, depending on what side of the bilayer interactions take place from.

In a novel use of this interaction Gopalakrishnan et al.[13] created liposomes with CdSe quantum dots in the bilayer, for applications in *in vivo* imaging. Quantum dots are interesting probes for imaging as they are not prone to photobleaching, whereas most organic dyes in use readily photobleach. The quantum dots were made hydrophobic by

coating with an organic ligand, trioctylphosphine oxide (TOPO). Two different hybrid vesicles were constructed, one for internalization into the cell, and another designed to fuse to the cell membrane. The resulting images are excellent examples of the potential of this technique for use in biomedical applications.

A nanoparticle may also interact with a lipid bilayer in a transient, traversing manner. A particle crossing the bilayer will create a transient defect, or a pore, in the membrane through which other particles, solvent, or solutes may subsequently pass. Nanoparticles have been documented to permeate cell membranes. Originally thought to permeate solely through endocytosis[17], whereby the entering particle is enveloped by the cell membrane, recent studies have shown that nanoparticles may also enter the cell by causing defects such as hole formation[18] (Figure 1.2C). This has been confirmed in *in vivo* studies by various groups [19, 20]. Most recently, Leroueil et al.[18] conducted studies on the defects induced in supported bilayers by a number of cationic nanoparticles. Supported bilayers were first formed on a mica surface, and subsequently exposed to an aqueous solution of the nanoparticles. All of the nanoparticles thus tested were effective at enhancing defects in the bilayer. The authors tested both organic nanoparticles [proteins and polyamidoamine (PAMAM)] dendrimers and inorganic nanoparticles such as gold and silicon core nanoparticles. It was found that nanoparticles could either a) aggregate on the bilayer without defect induction, b) expand existing defects, or c) directly induce defects in the lipid bilayer. This is notable because it means that only the particles that directly induce defects into the lipid bilayer are capable of permeating cell membranes via defect induction. Among the particles tested, amine-capped gold and silica nanoparticles demonstrated this capacity.

While these studies confirm the possibility of defect formation, they do not completely eliminate the endocytic pathway for entering cells. These studies were conducted on supported bilayers, where no transport proteins are present. As important as the results here are, the imaging techniques, atomic force microscopy (AFM), used by Leroueil et al.[18] do not provide much insight into the defect-inducing mechanism. If the defect is created by envelopment of the nanoparticle, as is done in endocytosis (predicted theoretically by Ginzburg and Balijepalli[11]), a continuous bilayer could be reformed if the two ends of the defect came into contact. Recent work by Verma *et. al*.[21] showed that novel gold nanoparticles, whose ligands, one hydrophobic (1-octanethiol) and another hydrophilic (11-mercapto-1-undecansulphonate) phase separate into bands of hydrophobic and hydrophilic regions (Figure 1.4). These nanoparticles avoid endocytosis, and penetrate the cell membrane.

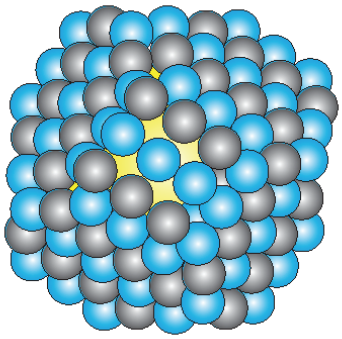

Figure 1.4: Schematic representation of phase-separated ligands on a nanoparticle. Blue represents a hydrophilic ligand while grey represents a hydrophobic ligand.

This phenomenon is believed to originate from the ordered structure of the ligands. Indeed, earlier experiments carried out on liposomes by Goodman *et. al*[22]., show that particles which contain both hydrophobic and hydrophilic ligands cause pore

formation in liposomes, although at the time of that publication, the phenomenon of phase separation of the ligands had not yet been invoked.

1.2.2 Membrane Transport

A simple way to test for the possibility of the interaction of a substance with a lipid bilayer is through a liposome leakage assay. In such an assay, liposomes are formed in a solution of a self quenching fluorophore, a compound whose fluorescence is quenched at high concentration, but is regained when the concentration is reduced beyond a certain threshold. This solution can then be purified to remove most of the un-entrapped dye, either by column chromatography or dialysis. The fluorescence of the liposomal solution is then monitored in the presence of the membrane active agent in question. If an increase in fluorescence is observed, it is concluded that the dye has leaked into the solution surrounding the liposome (Figure 1.5).

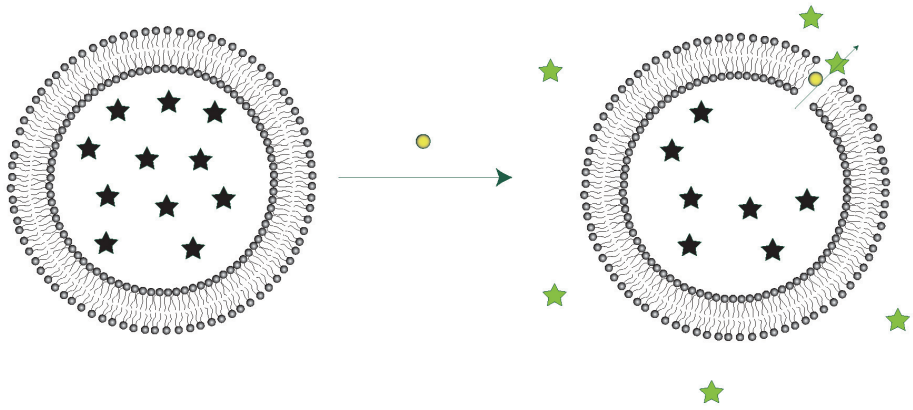

Figure 1.5: Schematic representation of a liposome leakage assay. The black stars represent a non-fluorescent, self quenched form of the dye and the green stars are a fluorescent form of the dye.

In order to distinguish the type of interaction from such an assay, an appreciation of the transport properties of lipid membranes is necessary. In a leakage assay as described, what is being monitored is the transport of a dye across the lipid membrane. To discern the interaction of the substance by such a parameter it is necessary to determine the mode

of transport which allows the dye to flow across the membrane. Membrane transport can be divided into three main categories:

1) general solubility-diffusion through a lipid bilayer

2) carrier mediated transport across the bilayer

3) pore mediated transport

Solubility diffusion occurs when a substance is soluble enough *in* the bilayer to readily pass through the membrane. In the case of a leakage assay, this can be ruled out, as dyes are selected for their ability to remain entrapped. Carrier-mediated transport is the crossing of a substance across the bilayer by a mobile molecule which serves as a shuttle. In this model, the mobile carrier and the permeant will form a complex which is translocated across the membrane, after which the permeant is released. Lastly pore mediated transport occurs when a membrane disruptant is affixed to membrane, creating a hole, by which a traversing particle may enter. In a nanoparticle liposome system, the last two mechanisms can be considered as plausible mechanisms for dye transport.

1.3 NANOPARTICLE-CELL INTERACTIONS

As previously alluded to, a nanoparticle crossing the cell membrane is not limited to direct interaction between the incoming particle and the lipids in the cell membrane. Cellular internalization may take place via one of the many mechanisms specifically designed for this purpose. In order to fully understand the mechanisms through which nanoparticles interact with cells, a complete understanding of both nanoparticle-lipid membrane interactions and *in vivo* nanoparticle cell interactions must be undertaken.

1.3.1 Cell Penetrating and Targeting Peptides

There remain many unknown factors regarding the cellular uptake and intracellular fate of nanoparticles. Despite lingering questions, numerous strategies have been developed to facilitate cellular uptake and even to localize incoming particles to specific regions within the cell. A successful, commonly employed strategy to tailor nanoparticles in this fashion utilizes cell-penetrating peptides (CPPs). The delivery of "cargo" using CPPs typically occurs though a process called endocytosis, the folding in of the cell membrane within itself to create a vesicle that is brought into the cell (Figure 1.7). Endocytosis may not be the only translocation mechanism, as it has been suggested that certain CPPs may cross though direct translocation of the lipid membrane[23]. Endocytic uptake is merely the first process in localizing a molecule to the desired target, as cargo may remain trapped in the endosome, the resulting vesicle of endocytosis (Figure 1.2B). In addition, it has recently been shown that proteases in the endosome can be responsible for nanoparticle degradation[24]. Much of the current targeted cell delivery science seeks to release endosomal molecules for further targeting.

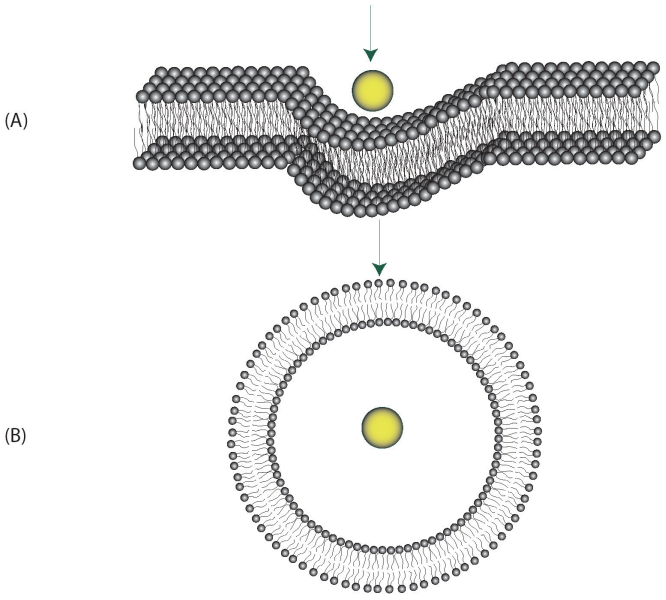

Figure 1.6: Schematic representation endocytosis.

In the absence of CPPs certain types of nanoparticles will be internalized by the cell while others may not. For instance, citrate-capped gold nanoparticles are known to be readily incorporated while polyethylene glycol (PEG) capped gold nanoparticles show little uptake[23]. The origin of this effect has been linked to the adsorption of serum proteins to the surface of the nanoparticles[24]. Alaadin *et. al.* found that regardless of the original surface charge, gold nanorods retain the same zeta potential in solution after exposure to bovine serum albumin (BSA). The authors reason that the possible uptake mechanism of the nanorods is receptor-mediated endocytosis, caused by the recognition of particle adsorbed proteins by membrane receptors. This correlates to previous findings, that BSA does not adsorb as strongly to PEG modified silicon surfaces[25] than unmodified silicon.

For these reasons CPP modified nanoparticles have become a convenient scaffold through which to introduce biological agents into the cell, but also a means by which the

uptake mechanism can be studied, as certain CPPs may promote internalization using one of, or several, known uptake mechanisms. The first CPP to be discovered was the Tat peptide. First discovered to aid in the internalization and replication of Human Immunodeficiency Virus 1 (HIV-1) in 1988[26], Tat is certainly the most commonly used CPP today. The region of the protein which consists of Tat, the transactivator of transcription (Tat) region, has 86 amino acids and consists of three functional domains. The first region, an acidic region, is responsible for transactivation, or increasing the rate of gene expression in the viral host. The second region is a cysteine rich region (10-15 amino acids in length, depending on the strain), serves as the DNA-binding region. The last region, a basic domain, aids in the nuclear import of the virus[27]. Although certain HIV-1 strains may carry a Tat peptide up to 102 amino acids long, many of the Tat CPPs used today are much shorter derivatives of the original protein. Peptides of 10-12 amino acids are typically implemented. Being composed of multiple arginine residues, the Tat peptide is polycationic. It is this concentration of positive charges which is thought to aid in cellular uptake. Internalization is typically thought to proceed thought endocytosis, though the full mechanism of Tat uptake is unknown, and many studies report varying results. Initial attempts to determine the uptake mechanism confirmed an endocytic pathway[27], though more recent results suggest otherwise[28-30]. For example, recent experiments, conducted at 4°C, where endocytosis cannot occur, have shown significant uptake of cargo[28]. Though endocytosis has not been discarded as a mechanism, it seems that it may not be the only pathway responsible for Tat internalization. The various size and shapes of the Tat conjugates used in these experiments may suggest a morphological dependence on the uptake[30]. Other commonly used CPPs, such as adenoviral RME, and

integrin binding domains (IBDs), can also bind receptor proteins, stimulating endocytic internalization[31].

Despite the ambiguity in the uptake mechanism involved in Tat internalization, the peptide has found widespread use a cellular delivery agent. As a CPP for nanoparticles, endosomal uptake remains a problem, as harsh conditions such as low pH and various proteases can break down the ligands. Fortunately this can often be averted using a mixture of other targeting peptides. An elegant yet simple way to avoid degradation and trapping by endosomes is to exploit the endosomal disruptive properties of the peptide HA2. HA2 is derived from influenza hemagglutinin (HA), the protein responsible for binding the influenza virus to the host cell. When subjected to low pH, as in endosomes, the conformational changes that HA experiences allows the influenza lipid envelope to fuse to the endosomal membrane, in turn permitting the virus to enter into cytosol[32].

Once molecular cargo, such as nanoparticles, leaves the endosome, it can then be targeted to specific regions in the cell. Specifically, the nucleus remains an important target, as new methods for gene delivery become more widespread. A series of peptides, known as nuclear localization signals (NLSs), exist precisely for this purpose. NLSs act by binding to carrier proteins, after which they will cross the nuclear membrane via an active transport mechanism[33]. Conveniently, commonly used Tat peptide sequences typically contain a string of peptides that may act as a NLS. Other NLS peptides are derived from adenoviral, or simian virus (SV40) proteins.

1.3.2 Nanoparticle-peptide Conjugates

The aforementioned tunable surface chemistry of nanoparticles allows for the addition of targeting peptide ligands. Indeed, various protocols have been used to functionalize peptides to nanoparticles[34-36]. Nanoparticles offer the added advantage that multiple targeting ligands can be added to the same nanoparticle. Multi-targeted nanoparticles can therefore be tailored to bypass the most complicated of cell defenses.

The nucleus, containing the genetic information and the transcriptions machinery of the cell, is perhaps the most desirable cellular target. Unfortunately, despite the breadth of information available to facilitate such targeting, tailoring nanoparticles for nuclear delivery has been met with mixed success. Nanoparticle-peptide formulations that seem to work in one case often do not work in another. Gold nanoparticles functionalized with an NLS can be localized to the nucleus when a microinjection technique is used to introduce the particles into the cell[37]. Important in confirming the validity of NLS functionalized gold nanoparticles, such a direct injection of particles into the cell, does not represent the entirety of cell processes an incoming particle would be subjected to. In fact, experiments in which these same particles were introduced in the cell growth media, showed cytoplasmic-localized nanoparticles result, but no entry into the nucleus is observed. In an early example of successful nuclear delivery, Lewin *et. al.*[38] delivered ca. 45 nm Tat-derivatized iron oxide nanoparticles into the nucleus. Similarly promising results were obtained with a combination of an adenoviral RME peptide, and an adenoviral NLS functionalized gold nanoparticle[39]. Interestingly, when both of these peptides were attached to the particle in their native state, that is in a single peptide sequence, nuclear localization was found to be less effective. Work from the

same research group[40] has also shown that Tat-conjugated gold nanoparticles undergo efficient internalization but fail to reach the nucleus. At low temperature incubation, where endocytosis cannot take place, the particle-peptide conjugate ceased to internalize at all, suggesting endocytosis as the primary uptake mechanism. On the other hand, gold nanoparticles modified with a synthetic peptide containing an adenoviral NLS and an IBD, did exhibit endocytic uptake, as well as strong nuclear signals. Similar results were obtained when Tat-modified CdSe-ZnS core-shell quantum dots (QDs) were introduced into human embryonic kidney cells; QDs showed high cytoplasmic uptake, but were absent from the nucleus[36]. Conversely, Gao *et. al.*[41] obtained strong nuclear fluorescence from Tat-modified CdSe-ZnS core-shell QDs. Both of these studies used 5 nm core-shell particles, though the capping ligands differed dramatically. Delehanty *et. al.* used dihydroxylipoic acid (DHLA) to replace the normally hydrophobic trioctylphosphine oxide ligand hydrophilic, while Gao *et. al*. used an ABC triblock copolymer structure. Delehanty *et. al.* have suggested that the 5-6 nm diameter of the nanoparticles is too large to enter the nuclear pore complex, whose diameter is 5 nm. However the QD complex successfully used by Gao *et. al.* had a hydrodynamic radius of 15nm. While the nuclear pore complex diameter may certainly limit the crossing of substances, it does not seem to be the only factor involved. 13 nm gold nanoparticles functionalized with Tat or NLS, and antisense oligonucleotides (meant to slow the expression of a protein) showed considerable gene knockdown, suggestive of nuclear accumulation. The same peptide antisense gold nanoparticles, when fluorescently labeled, showed distinct nuclear fluorescence as well[42]. The potential of using gold nanorods for nuclear targeting has also been investigated. NLS conjugated gold nanorods, approximately 40 nm in length, with

an aspect ratio of 2.4 (eg. 40 x 14 nm) demonstrated localization in both the cytoplasm and nucleus, as imaged by dark-field scattering microscopy. Finally, in an attempt to characterize the factors determining the degree of nuclear localization, Liu and Franzen[43] tested three targeting peptides. Adenoviral RME, NLS, and an integrin binding domain were attached to both gold nanoparticles and quantum dots, for use as delivery agents for antisense oligonucleotides. As a control, the oligonucleotide was also delivered directly to the cytoplasm, via a transfection agent, the cationic lipid mixture marketed as Lipofectin®. This lipidic transfection agent can be used to directly introduce cargo into the cell, by fusing to the cell membrane thereby avoiding endocytosis. The gold nanoparticle-peptide system showed significantly less nuclear activity than the Lipofectin®-oligonucleotide control. However, when the nanoparticles were also introduced using Lipofectin®, more activity was found than the control. Without the use of targeting peptides, the QD showed less activity than the nanoparticles. Considering this data, Liu and Franzen suggest that the nanoparticle conjugates are extremely susceptible to cellular degradation, particularly in the endosome.

1.4 CONLUDING REMARKS AND OUTLINE OF THESIS

As can be inferred from the information above, much remains to be elucidated concerning the interactions of ligand capped gold nanoparticles with lipid bilayers. This problem is particularly relevant, as lipid bilayer-nanoparticle interactions constitute the first contact incoming particles will experience with living cells. This thesis is dedicated to furthering the understanding of the mechanism and the factors contributing to this problem. It is divided into three experimental chapters each addressing an individual problem concerning this issue.

References

1. Corr, S. A.; Byrne, S. J.; Tekoriute, R.; Meledandri, C. J.; Brougham, D. F.; Lynch, M.; Kerskens, C.; O'Dwyer, L.; Gunko, Y. K. *J. Am. Chem. Soc*., **2008**. 130(13), 4214-4215.

2. Loo, C.; Lowery, A.; Halas, N; West, J.; Drezek, R. *Nano Letters*, **2005**. **5** (4), 709 -711.

3. Paciotti, G. F.; Kingston, D. G. I.; Tamarkin, L. *Drug Development Research,* **2006**. 67, 47-54.

4. Gorter. E.; Grendel, F. *Journal of Experimental Medicine*, **1925**, 41, 439-443.

5. Singer, S. J.; Nicolson, G. L. *Science*, 1972, 175, 720-731.

6. Engelman, D.M. *Nature,* 2005, 438 (7068), 578-580.

7. Zhang, L.; Granick, S. *Nano Letters*, 2006, 6 (4), 694-698.

8. Tohver, V.; Chan, A.; Sakurada, O.; and . Lewis, J. A. *Langmuir*, 2005. 17, 8414.

9. Yu, Y.; Anthony, M. A.; Zhang, L.; Bae., S. C.; Granick, S. *J. Phys. Chem. C.*, **2007**, 111, 8233-8236.

10. Urban, A.S.; Fedoruk, M.; Horton, M. R.; Rädler J. O.; Stefani, F. D.; Feldmann J. *Nano Letters,* **2009**, 9 (8), 2903-2908.

11. Ginzburg, V. V.; Balijepalli, S.; *Nano Letters*, **2007**, 7 (12), 3716-3722.

12. Noguchi, H.; Takasu, M. *Biophysical Journal,* **2002**, 83, 299-308.

13. Gopalakrishnan, G.; Danelon, C.; Izewska, P.; Prummer, P.; Geissbhler, I., Dubochet, J.; Vogel, H. *Angew. Chem. Intl. Ed.,* **2006**, 45, 5478-5483.

14. Jang, H.; Pell, L. E.; Korgel, B. A.; English, D. S., *Journal of Photochemistry and Photobiology A: Chemistry*, **2003,** 158, 111-117.

15. Binder, W. H.; Sachsenhofer, R.; Farnik, D.; Blaas, D. *Physical Chemistry Chemical Physics*, **2007**, 9, 6435-6441.

16. Paasonen, L.; Laaksonen, T.; Johans, C.; Ylperttula, M.; Kontturi, K.; Urtti, A. *Journal of Controlled Release*, **2007**, 86-93.

17. Wilhelm, C.; Gazeau, F.; Roger, J., Pons, J. N.; Bacri, J. *Langmuir*, **2002,** 18, 8148-8155.

18. Leroueil, P. R.; Berry, S. A.; Duthie, K.; Han, G., Rotello V. M.; McNerny, D. Q.; Baker Jr. J. R.; Orr, B. G.; Holl, M. M. B. *Nano Letters*, **2008,** 8 (2), 420-424.

19. Lerouil, P. R.; Hong, S. Y.; Mecke, A.; Baker, J. R.; Orr, B. G.; Holl, M. M. B. *Accounts of Chemical Research,* **2007**, 40 (5), 335-342.

20. Monteiro-Riviere, N. A.; Nemanich, R. J.; Inman, A. O.; Wang, Y. Y.; Riviere, J. E. *Toxicology Letters*, **2005**, 155 (3), 377-384.

21. Verma, A.,; Uzun, O.; Hu, Y.; Han, H. S.; Watson, N.; Chen, C.; Irvine, D.; Stellacci, F. *Nature Materials*, **2008**, 7, 589-595.

22. Goodman, C. M.; McCusker, C. D.; Yilmaz, T.; Rotello, V. M. *Bionconjugate Chemistry*, **2004**, 15, 897-900.

23. Nativo, P.; Prior, I. A.; Brust, M. *ACS Nano*, **2008**, 8, 1639-1644.

24. Alaadin M. A.; Nagaria, P. K.; Hexel, C. R.; Shaw, T. J.; Murphy, C. J.; Wyatt, M. D. *Small*, **2009**, 5 (6), 701-708.

25. Zhang, M.; Desai, T.; Ferrari, M. *Biomaterials*, **1998**, 19, 953-960.

26. Wagstaff, K.; Jans, D. A. *Current Medicinal Chemistry,* **2006**, 13, 1371-1387.

27. Lindgren, M.; Hällbrink, M.; Prochiantz, A.; Langel, Ü. *Trends in Pharmacological Research*, **2000**, 21, 99-103.

28. Mann, D. A.; Franklin, A. D.; *EMBO J*., **1991**, 10, 1733-1739.

29. Gumbleton, M.; Abulrob, A.G.; Campbell, L. *Pharm. Res*., **2000**, 17, 1035-1038.

30. Langel, Ü. *Cell Penetrating Peptides: Process and Applications*, CRC Press: Boca Raton: 2002.

31. Wu, E.; Nemerow, G. *Trends in Microbiology*, **2004**, 12, 162-169.

32. Hernandez, L.D.; Hoffman, L.R.; Wolfsberg, T.G.; White, J.M. *Annu. Rev. Cell Dev. Biol.,* **1996**, 12, 627–661.

33. Rout, M.P.; Blobel, G.; Aitchison, J.D. *Cell*, **1997**, 89, 715-725.

34. Kumar, S.; Aaron, J.; Sokolov, K. *Nature Protocols*, **2008**, 3, 314-320.

35. Sun, L.; Liu, D.; Wang, Z. *Langmuir*, **2008**, 24, 10293-10297.

36. Delehanty, J. B.; Medintz, I. L; Pons, T.; Brunel, F. M.; Dawson, P. E.; Matoussi, H. *Bioconjugate. Chem.,* **2006**, 17, 920-927.

37. Feldherr, C. M.; Akin, D. *J. Cell Biol.*, **1990**, *111*, 1-8.

38. Lewin, M.; Carlesso, N.; Tun, C-S.; Tang, X-W.; Cory, D.; Scadden, D. T.; Weissleder, R. *Nature Biotechnology*, **2000**, 18, 410-414.

39. Tkachenko, A. G.; Xie, H.; Coleman, D.; Glomm, W.; Ryan, J.; Anderson, M. F.; Franzen, S.; Feldheim, D. L. *J.Am.Chem.Soc*., **2003**, 125, 4700-4701.

40. Tkachenko, A. G.; Xie, H.; Liu, Y.; Coleman, D.; Ryan, J.; Glomm, W.; Shipton, M. K.; Franzen, S.; Feldheim, D. L. *Bioconjugate Chem*., **2004**, 15, 482-490.

41. Gao, X.; Cui, Y.; Levenson, R. M.; Chung, L. W. K.; Nie, S. *Nature Biotechnology*, **2004**, 22, 969-976.

42. Patel, P. C.; Giljohann, D. A.; Seferos, D. S.; Mirkin, C. A. *Proc. Natl. Acad. Sci.,* USA, **2008**, 105, 17222-17226.

43. Liu, Y.; Franzen, S. *Bioconjugate Chem.*, **2008**, *19* (5), 1009–1016

CHAPTER 2

Incorporation of Gold Nanoparticles into Phospholipid Bilayers

2.1 INTRODUCTION

Understanding the individual mechanisms through which a nanoparticle can interact with a lipid bilayer, as discussed in section 1.2, is not only important for studies of membrane mimics, but also for use in the development of novel materials. Combining the unique properties of materials confined to the nanoscale, and the biocompatibility of lipids has the potential to yield specialized nano-conjugates. The type of interaction pictured in Figure 1.2B, is of particular interest for use in biological systems, as the nanoparticle's movement is restricted to be within the bilayer. Such restricted movement of the nanoparticle is likely to significantly reduce the toxicity. Similar materials have in effect been described experimentally, using various nanoparticles. Gopalakrishnan *et. al.*[1] for example, produced convincing images of such CdSe quantum-dot liposome hybrids. On the other hand the images of liposomes prepared with gold[1,2] and silver[3] nanoparticles remain inconclusive. For these reasons the incorporation of several ligand-capped gold nanoparticles into the lipid bilayers of liposomes was attempted here. The following section is a description of experiments undertaken to meet this goal.

2.2 MATERIALS

All lipids used were purchased from Avanti Polar Lipids (Alabaster, AL): Fluorescent lipid, *N*-(6-tetramethylrhodaminethiocarbamoyl)-1,2-dihexadecanoyl-*sn*-glycero-3-phosphoethanolamine, triethylammonium salt (TRITC-DHPE), was purchased from Invitrogen Canada Inc. (Burlington, ON); hydrogen tetrachloroaurate ($HAuCl_4$) was

purchased from Strem Chemicals Inc. (Newburyport, MA). All other chemicals were purchased from Sigma-Alrich Canada (Oakville, ON) unless otherwise noted.

2.3 METHODS

2.3.1 Nuclear Magnetic Resonance (NMR) Spectroscopy

Nuclear Magnetic Resonance (NMR) spectra were acquired on a Varian 400 MHz ^{1}H instrument.

2.3.2 Transmission Electron Microscopy (TEM)

All transmission electron microscopy (TEM) images were obtained using a Phillips CM200 microscope using 200 kV accelerating voltage. Samples were prepared on 200 mesh carbon coated copper grids (SPI supplies, West Chester, PA). To prepare the liposomes for imaging, the liposome solution was dropped onto TEM grids that were placed on a metal puck, previously cooled in a liquid nitrogen bath for 5 minutes. The drop was allowed to sit until completely frozen after which the TEM grids were dried overnight in a vacuum oven at room temperature.

2.3.4 Confocal Microsopy

All confocal micrographs were obtained using a Zeiss LSM 510 META Confocal Microscope (Carl Zeiss AG, Germany) with an excitation wavelength of 488 nm and an emission wavelength of >505 nm wavelength.

2.3.5 UV-visible Spectroscopy

All UV-visible absorption spectra were obtained using a Cary 5000 UV-visible spectrophotometer (Varian, Inc. Walnut Hills, CA).

2.3.6 Fluorescence Spectroscopy

Fluorescence excitation spectra were recorded using a Cary Eclipse (Varian, Inc. Walnut Creek, CA) with a slit width of 5 nm.

2.3.7 Liposome Preparation

Small unilamelar vesicles were prepared using either the extrusion or sonication method. In the extrusion method liposomes were prepared as follows. Initially, 30 mg of 1,2-dimyristoyl-sn-glycero-3-phosphocholine (DMPC) was dissolved in 500 μL of $CHCl_3$ in a 4-mL vial. The chloroform was evaporated under a stream of N_2 while the vial was turned in order to form a thin lipid film on it walls. Any remaining $CHCl_3$ was removed under vacuum for at least 1 hour at room temperature. 3.0 mL of buffer (150 mM NaCl 10 mM Tris-HCl, .03% w/v NaN_3, pH adjusted to 8.5 with NaOH) was then added to the vial containing the lipid film. In the case of liposomes prepared in the presence of gold nanoparticles, the same buffer was prepared containing 20 mg of thioctic acid-capped gold nanoparticles. The colored solution contained large aggregates which were dissolved by vortexing, resulting in a red-colored turbid solution. The solution was filtered with a 0.45 μm hydrophilic syringe filter (Millipore, Etobicoke, ON) in order to remove any remaining lipid aggregates. The filtrate was collected and passed ten times through two stacked 100 nm polycarbonate filters in a Lipex extruder (Northern Lipids, Inc., Vancouver, BC). The vesicle-nanoparticle solution was purified with a Sephadex G-50 column. Fractions were collected from the column and characterized by UV-vis and TEM.

Liposomes prepared by sonication were prepared using the following procedure. 1.0 mL of a 1 mg/mL solution of 1,2-dioleoyl-*sn*-glycero-3-phosphatidylcholine (DOPC)

in chloroform was dried in a 5 mL round bottom flask using a rotary evaporator. When liposomes were formed in the presence of gold nanoparticles, the film was then re-dissolved in a 500 μL of a toluene solution of gold nanoparticles, and re-dried. The dried lipid solution was then further dried under vacuum at room temperature for at least 3 hours. In order to avoid TEM artifacts from salts, the lipid films were suspended in pure 18.2 mΩ MilliQ H_2O. After sufficient vortex mixing was performed so that no visible lipid film remained on the flask the solution was alternately sonicated, using a bath sonicator, and then vortexed for 10 seconds, three times each. The samples were then characterized using TEM.

2.3.8 Giant Unilamellar Vesicles (GUVs)

In order to immobilize the giant unilamellar vesicles (GUVs) for confocal imaging, GUVs were prepared using a mixture of lipids. A biotinlylated lipid, for immobilization,1,2-distearoyl-*sn*-glycero-3-phosphoethanolamine-N-[biotinyl (polyethyleneglycol)2000] (ammonium salt) (DSPE-PEG2000-biotin), and a fluorescent lipid, TRITC-DHPE, for imaging were added to the normal DOPC liposomes. In this formulation, 300 μL of 1 mg/mL DOPC, 10 μL, of 0.1 mg/mL DSPE-PEG2000-biotin, and 5 μL of 50 μg/mL TRITC-DHPE in chloroform were dried using a low argon stream on a Teflon plate. For nanoparticle-liposome preparations, the dried lipid film was re-suspended in 1 ml of toluene, and an aliquot of gold nanoparticles was then added. 1 ml of a 0.1 M sucrose solution was slowly dropped onto the Teflon plate, covered and allowed to swell overnight. Samples for imaging were prepared the following day in borosilicate microscope cells in which 500 μL of 0.5 mg/mL of freshly prepared avidin was pre-incubated for 15 min at room temperature. The cell was then washed twice with

0.1 M glucose and the GUVs were then added, and incubated for 5 min at room temperature to allow for biotin-avidin binding. The cell was then washed three times to remove unbound vesicles.

2.3.9 Gold Nanoparticle Preparation

A number of gold nanoparticle preparations were tried in order to tune the surface properties to appropriately interact with phospholipid bilayers.

Thioctic Acid Capped Gold Nanoparticles.

Thioctic acid capped gold nanoparticles were prepared according to the protocol developed by Rucareanu *et. al*[5]. In this procedure, thiotic acid capped gold nanoparticles are prepared by ligand exchange with N,N-dimethyl-4-aminopyridine (DMAP). The DMAP-capped gold nanoparticles are first prepared by dissolving 3.06 g tetroctylammonium bromide (TOAB) in 100 mL of toluene. 500 mg of $HAuCl_4$ was subsequently added in 30 mL of water. A fresh 25 mL aqueous solution of 525 mg of sodium borohydride ($NaBH_4$) was then added dropwise using a dropping funnel with a pressure equalizing arm while stirring. The reaction was allowed to proceed for ca. three hours. After washing with MilliQ water and drying over anhydrous sodium sulfate the TOAB-gold nanoparticle solution was added dropwise, using a dropping funnel with a pressure equalization arm and allowed to exchange overnight. The exchange is completed once the red-purple color of the toluene nanoparticle solution has moved to the lower aqueous phase. The lower aqueous phase is then removed. 20 mL of the aqueous DMAP gold nanoparticles is then added to 30 mL of 0.45 mM thioctic acid in 95% ethanol, and adjusted to pH 10 with KOH. The solid precipitate was then removed by centrifugation and the particles resuspended in acidic (pH 4) MilliQ water. The excess thioctic acid was

then removed by passing through a Sephadex G-25 column using acidic milliQ water as the eluant.

Alkanethiol-Capped Gold Nanoparticles

Gold nanoparticles protected with ligands of varying alkythiol chain lengths were synthesized according to a modified two phase Brust-Schiffrin[6] proccedure. In order to ensure that the nanoparticles were kept to a size smaller than the width of the bilayer, 4 nm, the gold:thiol ratio was adjusted according to the work of Hostetler *et. al*[7]. The Au:thiol ratio employed for the purposes of bilayer incorporation was 1:1. The resulting core diameter was 2.5±1 nm.

The particles were prepared by first dissolving 1.90 g of TOAB in toluene. 500 mg of $HAuCl_4$ was then added to the solution followed by the addition of just enough water to dissolve the gold salt. The alkanethiol was subsequently added and allowed to react for 15 min. 525 mg of $NaBH_4$ was then dropped in using a dropping funnel equipped with a pressure equalizing arm. The reaction was allowed to proceed for at least 3 hours before workup.

Effective cleaning was achieved by first separating the lower aqueous phase and washing 3 times with MilliQ water. The washed product was then evaporated to near dryness, using a rotary evaporator at 40°C; care was taken to ensure that no aggregates formed, but a minimum amount of solvent remained. The particles were then re-dispersed in a minimum amount of toluene (<15 mL) before being precipitated by the addition of ethanol. The precipitated particles were then rinsed three times with ethanol (ca. 50 mL per rinse) on a fritted glass filter funnel. It is important to ensure that the precipitated particles do not dry between washings, otherwise re-dispersion proves to be difficult.

After the ethanol washings, the precipitated particles were then dried by rinsing with acetone and allowing the particles to stand for ca. 15 min. The presence of free ligands was tested by ^{1}H NMR.

Tri-octylphosphine Oxide-Stearylamine Capped Gold Nanoparticles

Gold nanoparticles with a novel tri-octylphosphonium oxide (TOPO) and stearylamine mixed ligand shell were prepared according to the method reported by Green and O'Brien[8]. Briefly, 0.01 g of $HAuCl_4$ in 2 mL of 4-tert-butylpyridine was added to 2.0 g stearylamine, 5 g TOPO, and 0.00670 g of $NaBH_4$ at 160° C while stirring. The reaction was allowed to proceed for 30 minutes at 160° C. The reaction was then queched by precipitating the TOPO/stearylamine particles in methanol at 60° C. The precipitated gold nanoparticles were then washed by centrifugation four times. Particles were then filtered using a buchner funnel, rinsed with acetone and allowed to dry at room temperature. The dried powder was then re-dispersed in a minimum amount of toluene.

2.4 RESULTS

A number of gold nanoparticle formulations were assessed in order to gain an understanding of the factors ligand morphology and solubility play in influencing interactions with the lipid bilayers. While these factors will determine the region of the liposome a nanoparticle will associate with, to confidently ascertain this region remains difficult using conventionally available methods. The following section highlights results from the methods attempted.

2.4.1 Confocal Microscopy

The gold nanoparticles used in these experiments cannot be directly visualized using confocal microscopy, as the nanoparticles are significantly smaller than the

diffraction limit. In order for confocal microscopy to work as a technique to visualize the non-fluorescent gold nanoparticles, the fluorescence quenching properties of gold nanoparticles was exploited. For this purpose, liposomes were prepared with a fluorescent lipid, TRITC-DHPE, whose fluorescence a particle incorporated into the bilayer of the lipid vesicle would in turn quench. Preliminary studies into the quenching of the fluorescence by gold nanoparticles were undertaken (Figure 2.1). The experiment, carried out by the addition of hexadecanethiol ($C_{16}SH$) to a chloroform solution of TRITC-DHPE, shows that as the concentration of gold nanoparticles increases, the fluorescence of TRITC-DHPE is reduced, or quenched. Such a result confirms the feasibility of the confocal experiment. That is, a particle near or in the bilayer of a liposome should quench the TRITC-DHPE fluorescence image seen in a confocal image.

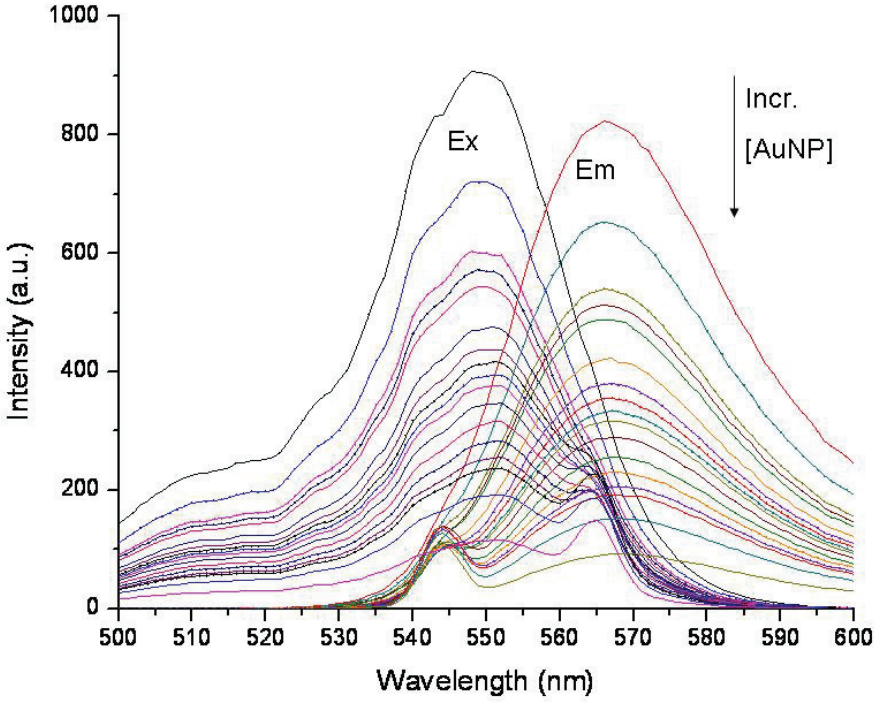

Figure 2.1: Fluorescence quenching due to gold nanoparticles.

Confocal images were collected for a number of ligand-capped gold nanoparticles. The gold-nanoparticle-liposome solutions imaged were dodecanethiol ($C_{12}SH$), hexadecanethiol ($C_{16}SH$), eicosanethiol ($C_{20}SH$), and tetraoctylphosphonium bromide capped particles. The resulting images obtained are shown, for the case of the $C_{16}SH$-capped gold nanoparticles, in Figure 2.2. On the left hand side is a control vesicle, formed without gold nanoparticles, on the right hand side is an image of vesicles formed in the presence of gold nanoparticles. The lack of a discernible difference between the two images implies that there is no incorporation into the bilayer. Such was the case for all of the previously mentioned nanoparticles.

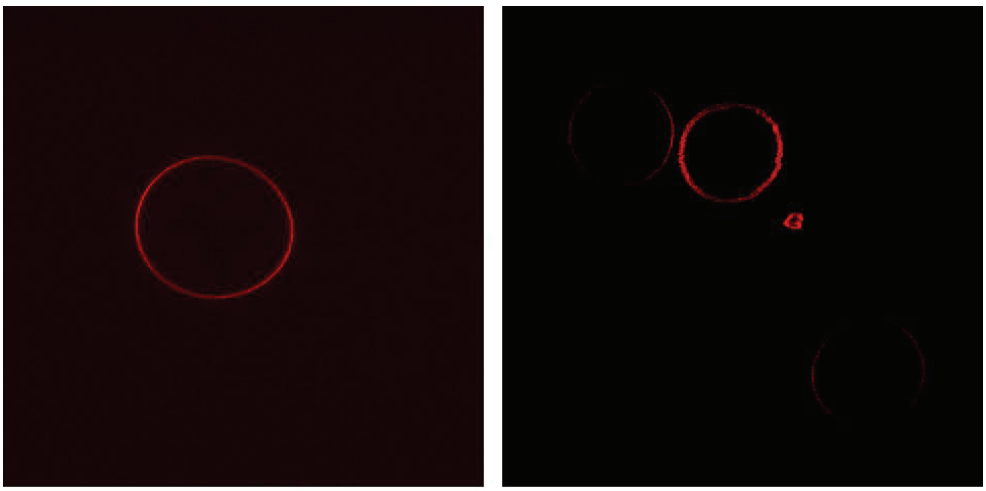

Figure 2.2: Confocal images of GUVs prepared without gold nanoparticles (left) and with gold nanoparticles (right).

2.4.2 Transmission Electron Microscopy

As opposed to confocal microscopy, transmission electron microscopy allows for direct visualization of gold nanoparticles. On the other hand, nanoparticles cannot be precisely localized to specific regions of a liposome. Furthermore when liposomes are prepared for imaging, the liposomes do not retain their structure. Liposomes prepared for imaging as described in Section 2.3.2 will collapse upon drying. Because of this, nanoparticles in, under, or on top of the liposome cannot be differentiated in a TEM image. Additionally, due to the lack of electron density of the lipids that make up a liposome, the contrast obtained from TEM imaging of liposomes is poor. Despite these limitations, TEM can still serve as an important tool for confirming or discounting association of a nanoparticle with a liposome. Figure 2.3 shows two separate samples of liposomes prepared with gold nanoparticles. Figure 2.3A shows liposomes prepared by extrusion with thioctic acid capped gold nanoparticles, while the liposomes in Figure 2.3B are prepared by sonication with hexadecanethiol-capped nanoparticles. Figure 2.3A shows a liposome strongly associated with the nanoparticles, while figure 2.3B shows the opposite, where nanoparticles tend to associate with other nanoparticles. The limitations imposed by TEM imaging as a method to determine the partitioning of nanoparticles in a liposome are illustrated in this figure. The nanoparticles imaged in Figure 2.3A show clear association with the liposome, but due to both the sample preparation and the image, nothing more can be definitely stated. In fact, although unlikely due to the clear circular arrangement of the nanoparticles, it could be argued that the nanoparticles could have serendipitously been deposited on the TEM grid in such a fashion under a liposome.

The aggregation displayed in Figure 2.3B could also be a result of the drying of the samples.

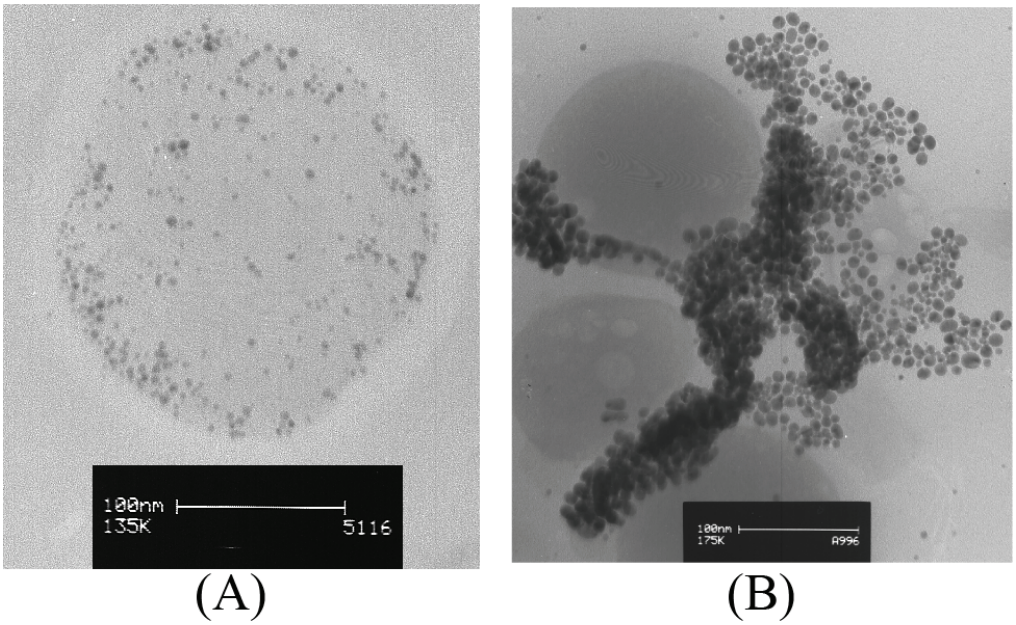

Figure 2.3: TEM images of gold liposomes prepared with thioctic acid-capped (A) and hexadecanethiol-capped (B) gold nanoparticles.

Similarly inconclusive results were obtained for the other nanoparticles prepared (Section 2.3.9). A final example, using dodecanethiol-capped nanoparticles, is shown in Figure 2.4. The results, analogous to Figure 2.3A, indicate liposomal interaction, but the exact mechanism cannot be deduced from the image alone. The results herein indicate that while TEM may not be capable of precisely pinpointing the location of a nanoparticle in a liposome matrix, it can serve to confidently discount association, such as shown in Figure 2.3B.

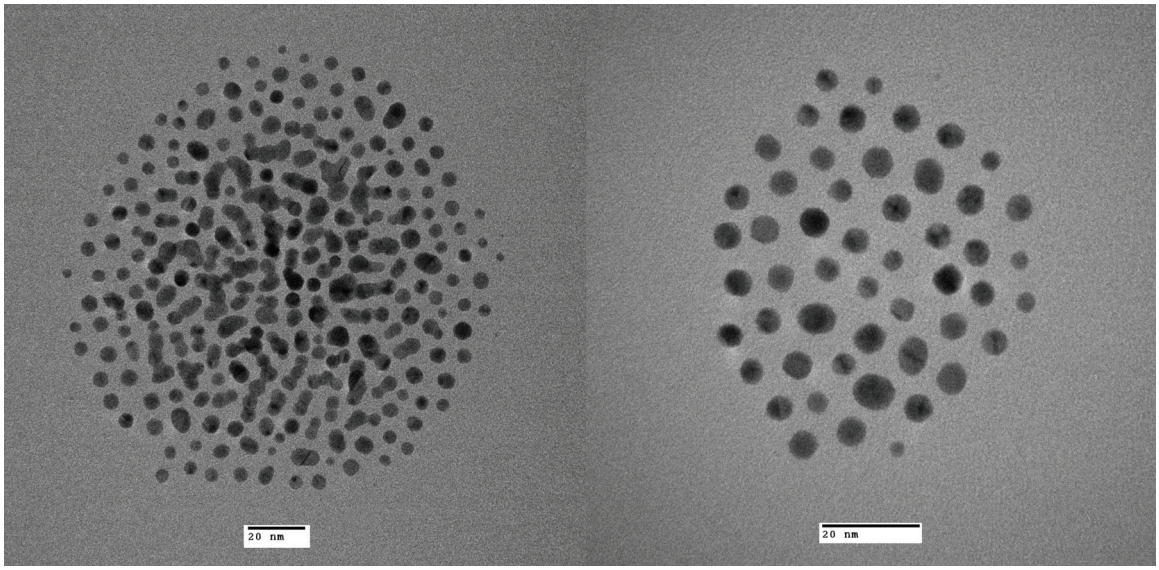

Figure 2.4: TEM images of liposomes prepared with dodecanthiol-capped gold nanoparticles

2.5 DISCUSSION

Sample preparation technique was shown to be critical in obtaining meaningful images by TEM. A liposome sample prepared for TEM by simply dropping the solution onto the grid and drying at room temperature retains little liposome morphology, as viewed by TEM. However, if the liposome solution was prepared as described in section 2.3.2, the images resulted in clear images of lipid vesicles, e.g. Figure 2.3. The exact reason for this distinction is unknown, but it can be reasonably speculated that freezing at liquid nitrogen temperatures helps retain the spherical structure during drying. Despite this advantage, gaining insight into the location of the nanoparticles in the liposome-nanoparticle preparations remained challenging.

The limitations imposed by the strategies employed do not however prevent helpful insight from being gained. From the collection of nanoparticles used and the images collected, the seemingly negative results give an idea of the complexity of the problem. It was presumed that the hydrophobicity of the ligand would determine the

location of the nanoparticle in or on the membrane. That is, liposomes prepared in the presence of nanoparticles with hydrophobic ligands would embed themselves into the bilayer, the only hydrophobic region of the bilayer (see Sections 1.1 and 1.2). The results obtained however seem to indicate that certain additional factors may be at play.

In preparing the liposomes with the alkanethiol-capped gold nanoparticles the original solutions showed little evidence for nanoparticle association. The images obtained were similar to those shown in Figure 2.3B. It was reasoned that the aggregation pictured was a result of the high concentration of nanoparticles used. Liposomes could not 'close' the bilayer with such high concentrations, essentially forcing the gold nanoparticles out of the bilayer. The liposomes were reformed using less concentrated samples but the results remain similar. Until the concentration of nanoparticles was so low that scarcely any particles were visible by TEM was this shown not to be the determining factor.

Another factor thought to affect the localization of nanoparticles within lipid membranes is the ligand structure. The fact that the most convincing report[1] to date showing the incorporation of nanoparticles in a bilayer used CdSe quantum dots capped with TOPO can perhaps be attributed to this ligand's structure. Although consisting of alkyl chains much like the alkanethiol ligands tested, the trivalent structure of TOPO may result in unique interactions with the alkyl chains of the lipids. Unfortunately, gold nanoparticles cannot be prepared with a ligand shell composed solely of TOPO. Mixed TOPO/stearylamine-capped gold nanoparticles were prepared according to the method developed by Green and O'Brien[8]. When imaged, by TEM, the particles showed no distinctive features indicating incorporation into the bilayer.

This collection of results indicate that the initial goal to partition gold nanoparticles into the lipid bilayers of liposomes was not achieved with unequivocal certainty. The results obtained in the process, however were critical in the development of an understanding of gold nanoparticle-lipid bilayer interactions. While the negative results obtained do not discount the possibility of an incorporative interaction, they do show that such an interaction is not determined strictly by hydrophobic/hydrophilic interactions. Even more critical to the development of the present Thesis was the conclusion that before undertaking the pursuit of specific interactions, it is crucial to establish whether or not gold nanoparticles will interact at all with lipid bilayers. This topic is explored in the following Chapter.

References

1. Gopalakrishnan, G.; Danelon, C.; Izewska, P.; Prummer, P.; Geissbhler, I.; Dubochet, J.; Vogel, H. *Angew. Chem. Intl. Ed.* **2006**, 45, 5478-5483.

2. Binder, H.W.; Sachsenhofer, R.; Farnik, D.; Blaas, D. *Phys. Chem. Chem. Phys.* **2007**, 9, 6435-6441.

3. Park, S.H.; Oh, S.G.; Mun, J.Y.; Han, S.S. *Colloid. Surf.* **2006**, 112-118.

4. Park, S.H.; Oh S.G.; Mun, J.Y.; Han, S.S. *Colloid. Surf. B.* **2005,** 44, 117–122.

5. Rucareanu, S.; Gandubert, V.J.; Lennox, R.B. *Chem. Mater*. **2006**, 18, 4674-4680.

6. Brust, M.; Walker, M.; Bethell, D.; Schiffrin, D.J.; Whyman, R. *Chem. Commun.* **1994**, 801-802.

7. Hostetler, M. J.; Wingate, J. E.; Zhong, C.J.; Harris, J.E.; Vachet, R.W.; Clark, M.R.; Londono, J. D.; Green, S. J.; Stokes, J. J.; Wignall, G. D.; Glish, G. L.; Porter, M. D.; Evans, N. D.; Murray, R. W.; *Langmuir*, **1998**, 14 (1), 17-30.

8. Green, M.; O'Brien, P. *Chem. Commun.* **2000**, 183-184.

CHAPTER 3

Gold Nanoparticle-Lipid Bilayer Interactions as Monitored by a Dye Leakage Assay

3.1 INTRODUCTION

Before a nanoparticle can become internalized into a living cell it must first come in contact with the cell membrane. After this initial contact the nanoparticle may enter through one of two or a combination of transport mechanisms (active transport, discussed in Section 1.2, or passive transport). Active transport of nanoparticles, particularly through endocytosis, is well documented (see Section 1.2), but little is known about the mechanism of nanoparticle-passive transport. Passive transport of gold nanoparticles has been demonstrated recently by Verma[1] *et. al.* In this report, gold nanoparticles with phase-separated ligands avoided endocytosis and entered the cell without disruption of the bilayers. Nanoparticles not having phase separated surface ligands, on the other hand, were endocytosed. The observation that ligand order and morphology can control the transport mechanism of nanoparticles in live cells is particularly interesting. If it is a general feature that these ligand characteristics determine nanoparticle transport, transmembrane nanoparticle transport might indeed be controllable. The detailed interactions between a nanoparticle and the lipid membrane are crucial as passive transport involves molecular interactions of incoming particles directly with the lipid bilayer.

The present Chapter summarizes experiments undertaken to explore this phenomenon. Multiple mixed ligand-capped gold nanoparticles were prepared with

varying order and morphology. Lipid bilayer-nanoparticle interactions were subsequently investigated using a liposome leakage assay adapted to the systems in question.

It is imperative that the liposomes used in the leakage assay be single unilamellar vesicles (SUVs). Leakage assays undertaken using multilamellar vesicles involve multi-compartment entrapment and very complex spectra and leakage kinetics. The leakage caused by a membrane disrupter would be greatly reduced as the incoming particle would be interacting with one vesicle at a time. For this reason it should be stated that in the course of this Chapter, the term liposomes refers strictly to small unilamellar vesicles.

3.2 MATERIALS

All lipids used were purchased from Avanti Polar Lipids (Alabaster, AL). All other chemicals were purchased from Sigma-Aldrich Canada (Oakville, ON) unless otherwise noted.

3.3 METHODS

3.3.1 Nuclear Magnetic Resonance (NMR) Spectroscopy

Nuclear Magnetic Resonance (NMR) spectra were acquired on a Varian 400 MHz ^{1}H instrument.

3.3.2 UV-visible Spectroscopy

All UV-visible absorption spectra were obtained using a double beam monochromator-based Cary 5000 UV-visible spectrophotometer (Varian, Inc. Walnut Hills, CA).

3.3.3 Fluorescence Spectroscopy

Fluorescent traces were recorded as a function of time using a Cary Eclipse (Varian, Inc. Walnut Creek, CA). An excitation wavelength of 495 nm and an emission

wavelength of 517 nm for 5(6)-carboxyfluorescein fluorescence was used. An emission wavelength of 515 nm for the case of calcein fluorescence was used (excitation was again at 495 nm). Aliquots of gold nanoparticles were added after approximately 15 minutes of observing the background fluorescence. Typically, 30 minutes after the particles were added a 20% w/w solution of SDS was injected into the cuvette in order to lyse the SUVs and release all remaining dye to the bulk solution. The times mentioned above are general, certain spectra were acquired at longer or shorter periods. The precise times can be discerned from the appropriate spectra.

3.3.4 Vesicle Preparation

SUVs were prepared by sonication, in a manner similar to that described in Section 2.3.7, using the following procedure. 1.0 mL of a 2.5 mg/mL lipid solution in chloroform was dried in a 5 mL round bottom flask using a rotary evaporator at least 5° C above the phase transition temperature of the lipid being used. The dried lipid solution was then further dried under vacuum at room temperature for at least 3 hours. The dried lipid film was then re-suspended in 100 mM 5(6)-carboxyfluorescein solution in phosphate-buffered saline (PBS, pH varied depending on experiment performed). Sufficient vortex mixing was performed so that no visible lipid film remained on the flask. The solution was then subjected to 5 freeze-thaw-sonicate cycles. The freezing was performed by immersion directly in liquid nitrogen by placing the round bottom flask in a beaker into a Dewar flask filled with liquid nitrogen. Sonication was performed using a Branson bath sonicator. The thawing step was performed in a water bath at least 10°C above the phase transition temperature of the lipid being used. The excess 5(6)-carboxyfluorescein was then removed with a Sephadex G-50 column, and the vesicles

were eluted in PBS at the experimental pH. Samples were assessed for lipid content by testing the fractions by silica thin layer chromatography and staining with molybdenum blue. Fractions that stained with molybdenum blue were deemed to contain phospholipids and were used in subsequent leakage assays. 10 μL of this solution was then diluted in 1990 μL of PBS in a fluorescence cuvette and allowed to equilibrate for at least 30 minutes before spectra were acquired. For reasons not completely understood, this equilibration step was found to be necessary in obtaining a stable, flat initial fluorescence signal (before adding nanoparticles).

3.3.5 Gold Nanoparticle Preparation

Gold nanoparticles with a mixed composition ligand shell were prepared according to the protocol developed by Rucareanu *et. al.*[2] Mixed monolayer gold nanoparticles are prepared by ligand exchange with N,N-dimethyl-4-aminopyridine (DMAP). The DMAP-capped gold nanoparticles are first prepared by dissolving 3.06 g tetroctylammonium bromide (TOAB) in 100 mL of toluene. 500 mg of $HAuCl_4$ (Strem Chemicals, Newburyport, MA),was subsequently added in 30 mL of water. A fresh 25 mL aqueous solution containing 525 mg of sodium borohydride ($NaBH_4$) was then added dropwise using a dropping funnel with a pressure equalizing arm, while stirring. The reaction was allowed to proceed for ca. three hours. After washing with MilliQ water and drying over anhydrous sodium sulfate the TOAB-gold nanoparticle solution was added dropwise, using a dropping funnel with a pressure equalization arm and allowed to exchange overnight. The exchange is completed once the red-purple color of the toluene nanoparticle solution has moved to the lower aqueous phase. The lower aqueous phase is then removed. 20 mL of the aqueous DMAP gold nanoparticles is then added to 30 mL of

0.45 mM thiol solution in 95% ethanol, and allowed to exchange overnight. A small amount of golden colored precipitate was observed after the exchange reaction was completed. In particle mixtures where precipitate was formed, the solid was removed by centrifugation and the nanoparticles re-suspended in the appropriate solvent, water or toluene. The volume of the nanoparticles was reduced using by rotary evaporation and the excess thiol was then removed by passing twice through a Sephadex G-25 column using MilliQ water as the eluant. Purity and ligand composition were verified by ^{1}H NMR. The purified gold nanoparticles could not be re-suspended in water after drying. However if the water contained a minimum amount of DMAP, re-suspension was immediate. Another interesting observation concerning the dried and purfied nanoparticles was the appearance of the nanoparticle film of particles prepared using a rotary evaporator. These films displayed a distinctive reflective, golden characteristic similar to that of bulk gold. This was not noticed if the particles were dried in an unpurified state.

3.4 RESULTS

3.4.1 Nanoparticle Characterization

Mixed monolayer-protected gold nanoparticles were prepared as per Section 3.3.5 using 11-mercaptoundecanoic (MUA) and 1-octanethiol (OT). The nanoparticles were synthesized using MUA percentages of 0, 25, 50, 75, and 100% in solution. After determining the ligand ratio using NMR, it was found that the capping ligand does not deposit onto the nanoparticle in the same ratio as in the solution. This is consistent with the large 2D RS-Au SAM literature concerning mixed SAM formation[3]. The NMR results are summarized in Table 3.1. The disparity between the solution ratio and the

nanoparticle ratio seem to indicate that the OT ligand displays a greater affinity for the nanoparticle surface than MUA.

% MUA in Solution	Percent MUA on Particle
0	0
25	18
50	37
75	66
100	100

Table 3.1: Percent MUA of purified gold nanoparticles as determined by NMR.

The gold nanoparticles were imaged by TEM in order to obtain sizing and morphology information. The sizing results are summarized in Table 3.2.

Particle	Particle Diameter
DMAP	4.8±1.9
18% MUA	4.6±1.0
37% MUA	6.0±.1.5
66% MUA	4.9±1.1
100% MUA	5.5±1.6

Table 3.2: Core diameter of gold nanoparticles used.

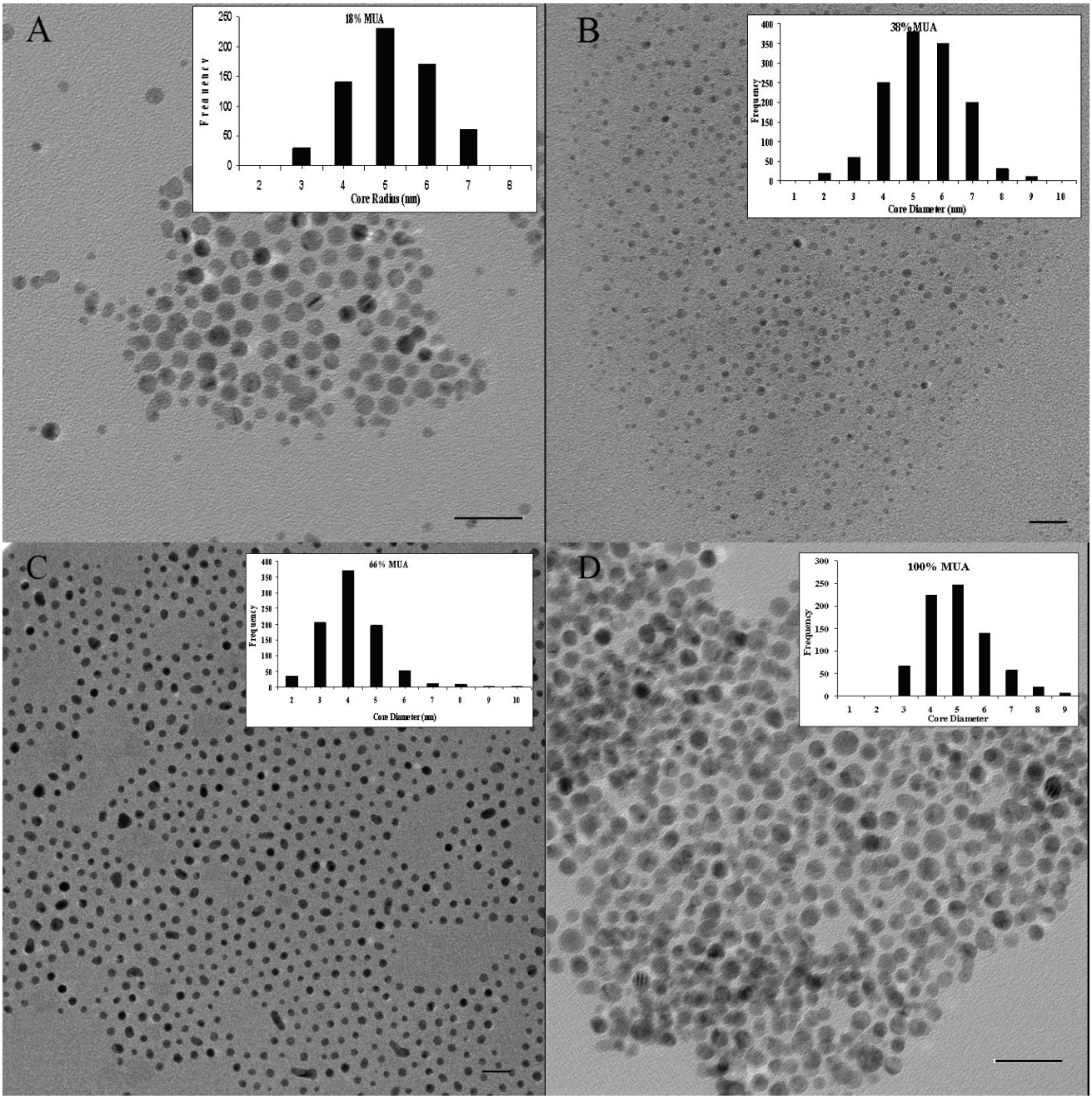

Figure 3.1: TEM images of 18% (A), 37% (B), 66% (C), and 100% (D) MUA gold nanoparticles. %MUA values are determined by ^{1}H NMR Insets show sizing histograms.

Further characterization was performed by UV-visible spectroscopy. Spectra were obtained for all of the water soluble MUA/OT-capped gold nanoparticles. The surface plasmon resonance peak maximum varied from 523 nm to 528 nm for the 37%-100%

MUA particles. The 18% MUA peak was drastically red-shifted, at around 550 nm. This presumably is due to aggregation as the 18% MUA capped gold nanoparticles are minimally soluble in water. The DMAP-capped nanoparticle surface plasmon resonance was centered around 520 nm.

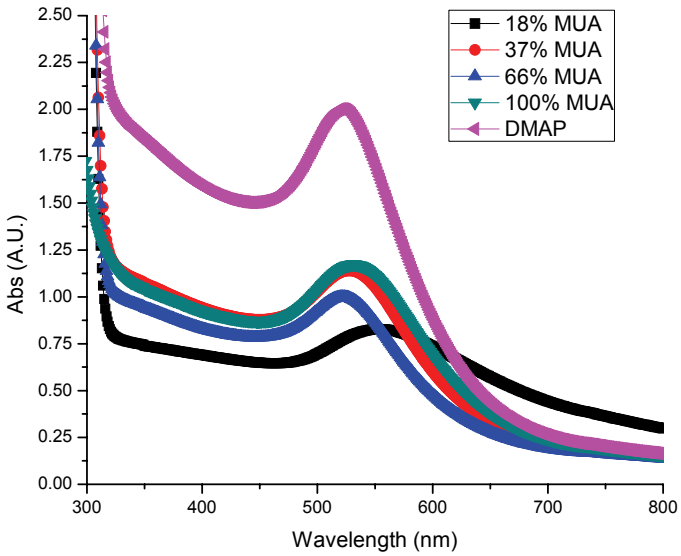

Figure 3.7: UV-visible spectra of DMAP and MUA/OT-capped gold nanoparticles.

3.4.2 Leakage Assay

The water soluble mixed, ligand capped gold nanoparticles characterized above, (37%, 66% and 100% MUA) were tested in the carboxyfluorescein fluorescence leakage assay described in Section 3.3.3. To test the effect of lipid composition and charge, each nanoparticle formulation was tested using neutral [1,2-dioleoyl-*sn*-glycero-3-phosphocholine (DOPC) and 1,2-dipalmitoyl-*sn*-glycero-3-phosphocholine (DPPC)], negatively charged [DOPC- 1,2-dioleoyl-*sn*-glycero-3-phospho-L-serine (DOPS)], and positively charged [DOPC-1,2-di-(9Z-octadecenoyl)-3-trimethylammonium-propane

(DOTAP)] lipid vesicles. Experiments with DOPC vesicles were also carried out at a range of pH values in order to assess the effect of the degree of MUA protonation has on the leakage induction. As a secondary control, a leakage assay was performed by substituting the 5(6)-carboxyfluorescein dye with another self-quenching dye, calcein.

The baseline fluorescence of the kinetic traces was taken as the intensity before adding nanoparticles to the solution. This value was subtracted from the subsequent increasing fluorescence to zero the fluorescence before particle addition. In cases when the addition of SDS did not increase the fluorescence beyond the saturation point of the detector, the final fluorescence value of the trace was taken as the point of complete leakage and fluorescence was plotted as percent leakage versus time. In equation form,

$$L_{\%} = \frac{I_t - I_0}{I_\infty - I_0} \times 100\% \qquad (1)$$

where $L_{\%}$ represents percent leakage, I_t is the fluorescence intensity at time t, I_0 is the zero value (taken as the fluorescence intensity just before the addition of nanoparticles), and I_∞ is the final value of fluorescence. In the case where SDS addition pushes the fluorescence off scale, the data was plotted as the corrected intensity, i.e. by plotting I_t minus I_0 versus time. For the purposes of comparison, an empirical term, L_{25}, is and defined as the percent leakage after 25 minutes.

In an effort to elucidate the dye transport mechanism, attempts were made to fit the kinetic data to first and second order kinetic rate laws. Adequate fits were not however obtained. Evidently the kinetics of the NP-induced leakage is more complex than the primary rate laws. As only certain regions of the kinetic fluorescence traces fit 1st or 2nd order kinetics it is likely that the leakage process may be a multi-exponential process.

The first leakage assays were conducted to quantitatively measure the leakage induced by the various water soluble mixed ligand-capped gold nanoparticles. The nanoparticles were added to neutral (zwitterionic) DOPC vesicles. The interaction of the nanoparticle with the lipid bilayer can be quantitatively correlated to the ligand composition and structure in this way. The results of this assay are shown in Figure 3.3. Interestingly it can be seen that the gold nanoparticles with the lesser quantity of MUA show the most leakage, suggesting the strongest interaction has occurred in the case.

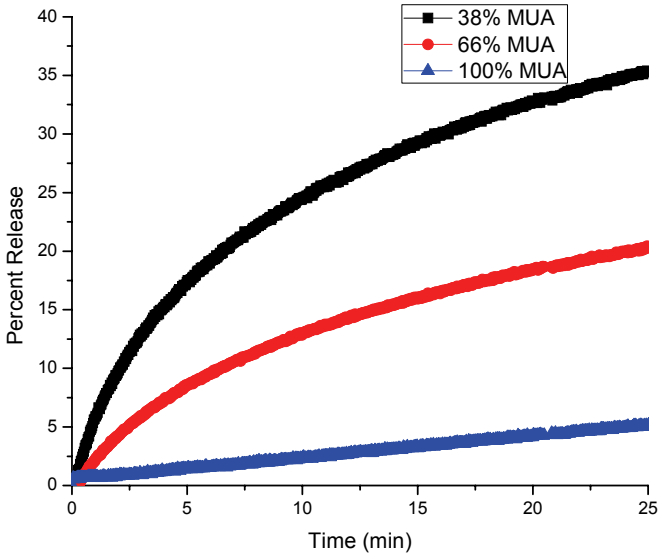

Figure 3.8: DOPC vesicle leakage assay performed with water-soluble gold nanoparticles at pH 7.

The 66% MUA capped gold nanoparticles were tested at various pH values not only to determine the effect of ligand protonation, but also to test the dye characteristics at different pH values. The initial leakage of the dye, that is, before adding particles, did not change significantly in the pH range tested (7.0-7.5). However, the leakage induced by the 66% MUA capped gold nanoparticles changes dramatically. The results, shown in Figure 3.3, show that after 25 minutes, the L_{25} changes nearly seven-fold.

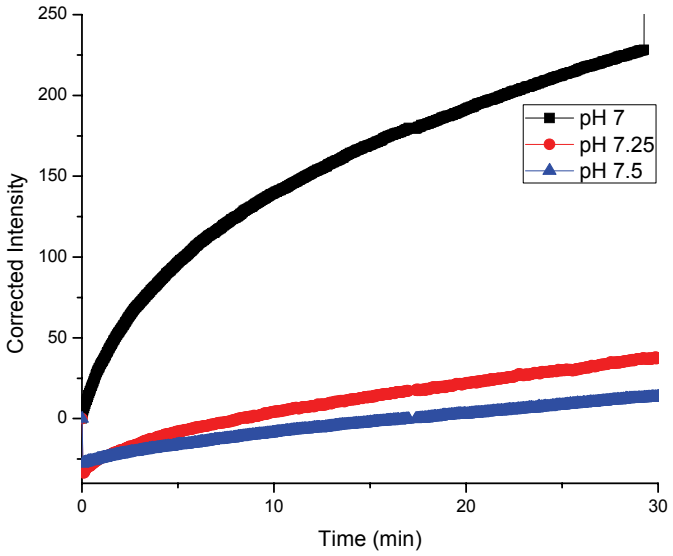

Figure 3.9: pH dependence of leakage induced by the 66% MUA-capped gold nanoparticles.

The MUA-capped gold nanoparticles were also tested using SUVs with an overall negative charge. DOPC SUVs were prepared with an overall 18% DOPS (negatively charged lipid) and the water soluble MUA-capped nanoparticles were added to this solution. The leakage caused by these particles is shown in Figure 3.5A. It is interesting to note that the trend seen in Figure 3.3 is reversed in this case. The 66% MUA-capped gold nanoparticles show the highest percent leakage, although the 38% MUA nanoparticles show a similar rate profile. Figure 3.5B shows the effect of increasing the DOPS concentration from 18% to 33% on the leakage effected by the 66% MUA nanoparticles. The opposite trend to what is expected is observed. By invoking simple charge arguments it can be reasoned that increasing the amount of negative charge on the vesicle should cause more repulsion, and thus less interaction, and less leakage. As shown in Figure 3.5B the reverse is in fact observed; increased vesicle anionic charge results in more leakage.

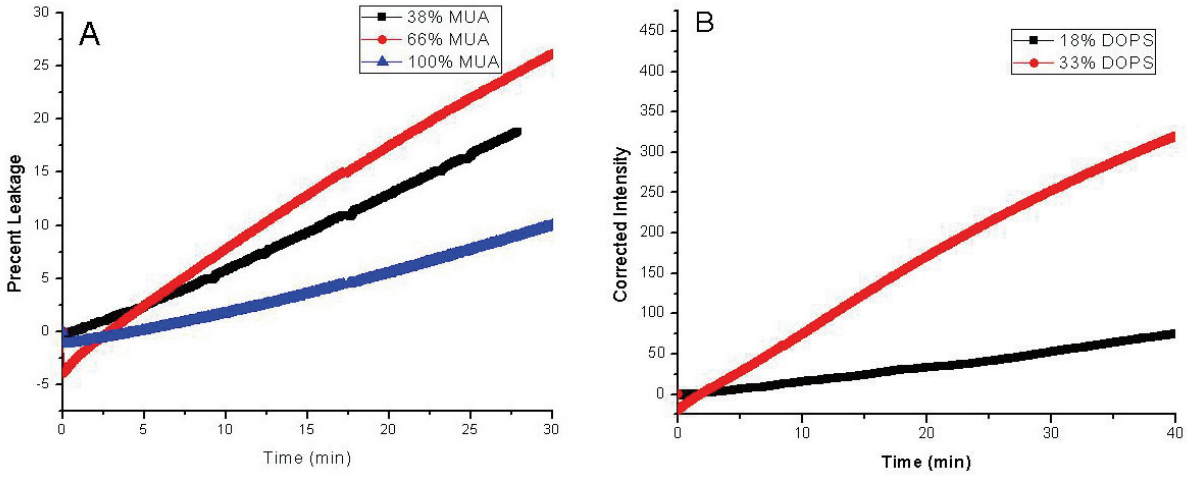

Figure 3.10: Leakage induced by gold nanoparticles in negatively charged SUVs. The water soluble nanoparticles were tested at varying anionic lipid contents of 18% (A) and 33% (B) to examine the effect of charge on the leakage process.

The water soluble gold nanoparticles were also assayed using positively charged DOPC vesicles, containing of 19% DOTAP. The results are summarized in Figure 3.6. The difference between the leakage process in the 66% and the 38% MUA-capped gold nanoparticles is minor in this case. In congruence with the previous leakage assays the 100% MUA-capped gold nanoparticles again exhibit less leakage than the other nanoparticle formulations.

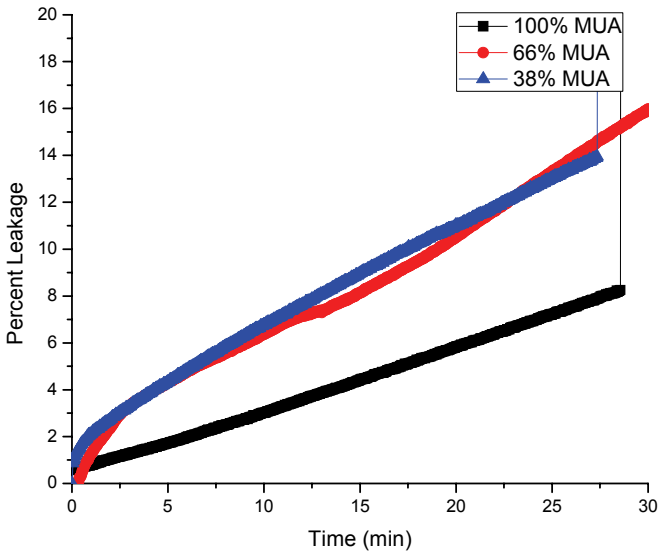

Figure 3.11: Cationic vesicles (19% DOTAP; 81% DOPC content) leakage induced by gold nanoparticles.

The assay was also carried out using an alternative dye, calcein (Figure 3.7A). Substitution with calcein ensures that the leakage described in the previous assay was not due to artifacts caused by the carboxyfluorescein dye itself. Finally, to demonstrate the possibility of extending the leakage assay to lipids which are not in the disordered liquid crystalline phase, the assay was performed using SUVs composed of DPPC, a lipid known to be in the gel phase at room temperature (T_m=41.4°C) (Figure 3.7B).

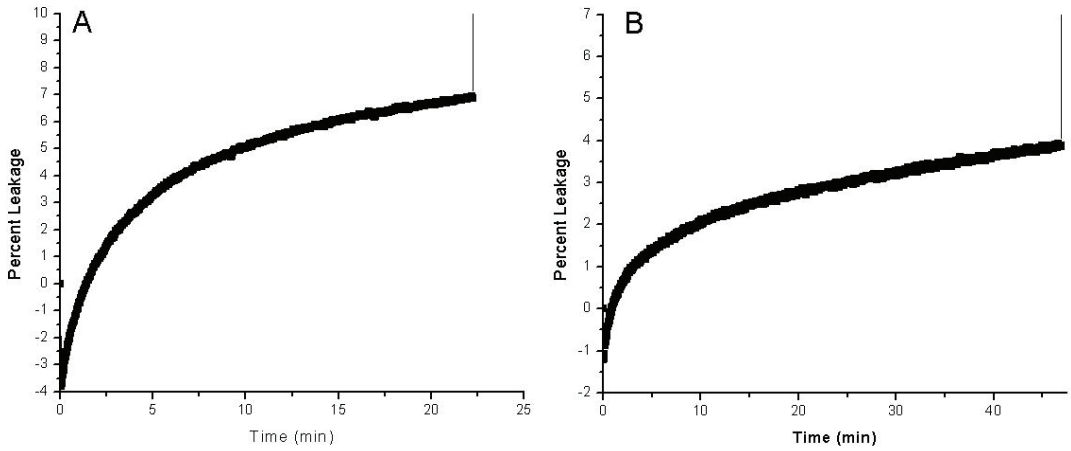

Figure 3.12: Vesicle leakage assay performed using calcein (A) and DPPC vesicles (B).

3.5 DISCUSSION

Small unilamellar vesicles can serve as a simple model of the cell membrane[4] in the absence of surface proteins. SUVs, as used in the leakage assay developed, provide a simple method to quantitatively study the interactions of membrane perturbants, including the gold nanoparticles studied here, with a cell membrane. The leakage assay was performed under a range of conditions to evaluate the factors contributing to the membrane perturbation when it is observed.

In the assay performed with neutral DOPC vesicles the results are contrary to cell work, reported by Verma *et. al.*[1], where they used a mouse dendritic cell clone DC2.4. According to a recent report[5] by the same group, gold nanoparticles in the size range of the particles used here, when prepared with a similar proportion of hydrophilic and hydrophobic ligands (38% MUA in the case of the aforementioned leakage assay) exhibit no phase separation of ligands on the nanoparticle surface. Their work showed that when exposed to live cells, such nanoparticles are internalized mostly by endocytosis, suggesting that no strong nanoparticle-membrane interactions occur. Conversely,

nanoparticles whose ligands were phase separated showed little or no cytoplasmic uptake, leading to the conclusion that gold nanoparticles with ordered/phase separated ligands are taken up into cells via passive uptake. As discussed in Section 3.1, passive uptake requires direct contact with the cell membrane. The results shown in Figure 3.3 using the model membranes described here demonstrate an opposite trend. At pH 7, the 38% MUA-capped gold nanoparticles show the greatest extent of leakage, whereas the 66% MUA-capped gold nanoparticles show significantly less leakage. The 100% MUA-capped nanoparticles show the least leakage under these conditions. This seems to indicate that the more hydrophobic a nanoparticle is, the stronger will be its interaction with a zwitterionic lipid bilayer.

Despite the trend shown in Figure 3.3, increasing the pH from 7.0 to 7.5 decreased the extent of leakage (Figure 3.4). The hydrophobic nature of the ligands is enhanced at low pH given that the surface pKa of the carboxylate is ca. 7. The trend in Figure 3.4 thus correlates with the findings presented in Figure 3.3. The change in protonation state can be a significant factor as ca. 50% of the MUA will be ionized at pH 7.0 and ca. 75% at pH 7.5. Such a small change in pH might dramatically change the leakage. The nearly seven fold increase in the L_{25}, however, implies that another factor might also determine.

When the leakage assay was performed using negatively charged (Figure 3.5A) vesicles the trend of the mixed monolayer-capped gold nanoparticles (38% and 66% MUA) is reversed when compared to the neutral vesicles (Figure 3.3). Considering that the 66% MUA-capped gold nanoparticles have a higher negative charge at pH 7, it should be expected that the increased electrostatic repulsion between the two like charges

will reduce the interaction of the nanoparticles with the lipid membrane. However the opposite effect is seen, as the L_{25} of the 66% MUA nanoparticles is greater than that of the 38% MUA nanoparticles and this is further confirmed in Figure 3.5B, where the increased negative charge on the vesicles leads to increased leakage. The increased leakage at higher negative charge indicates that repulsive interactions can lead to increased membrane disruption. When compared to positively charged vesicles (Figure 3.6) the L_{25} is less for all nanoparticle formulations tested, another indication that repulsive interactions cause further disruption. Nonetheless, in all cases tested (neutral, negative, and positive SUVs), the 100% MUA nanoparticles consistently exhibit a lower extent of leakage. Taking this point into account it appears that presence of the hydrophobic octanethiol ligands enhances the nanoparticle-bilayer interactions.

From the above observations it can be concluded gold nanoparticles are capable penetrating lipid bilayer, independent of energy-dependent transport mechanisms. While the exact mechanism of interaction is not known, 5(6)-carboxyfluorescein leakage assays indicate that ordered ligand morphologies may not be the dominant factor in influencing membrane disruption. Rather, the data demonstrate that the presence of simple hydrophic ligands, such as alkythiols enhances these interactions, and that the very specific ionization state of the nanoparticle is critical. A proper understanding of the interactions discussed requires nanoparticle interactions to be studied *in vivo*. This is the subject of the following Chapter.

References

1. Verma, A.; Uzun, O.; Hu, Y.; Han, H. S.; Watson, N.; Chen, C.; Irvine, D.; Stellacci, F. *Nature Materials*; **2008**, 7, 589-595.

2. Rucareanu, S.; Gandubert, V.J.; Lennox, R.B. *Chem. Mater*. **2006**, 18, 4674-4680.

3. Bain, C. D.; Troughton, E. B.; Tao, Y. T.; Evall, J.; Whitesides, G. M.; Nuzzo, R. G. *J. Am. Chem. Soc.* **1989**, 111, 321-335.

4. Jain, M. K. *The Bimolecular Lipid Membrane.* **1972**. New York: Van Nostrand Reinhold

5. Carney, R.P.; DeVries, G.A.; Dubois, C.; Kim, H.; Kim, J.Y.; Singh, C.; Ghorai, P.K.; Tracy, J.B.; Stiles, J.B.; Murray, R.W.; Glotzer, S.C.; Stellacci, F. *J. Am. Chem. Soc.* **2008**, 130, 798-799.

6. Vezenov, D. V.; Noy, A.; Rozsnyai, L. F.; Lieber, C. M. *J. Am. Chem. Soc.* **1997**, *19*, 2006.

APPENDIX A

Determination of Ligand Ratios by ^{1}H NMR Spectroscopy

The ligand ratio on the purified gold nanoparticles was determined using the methodology developed by Wang and Murray[1]. Briefly, approximately 50 mg of gold nanoparticles was dissolved in a minimum amount of solvent. 3-4 mg of iodine (I_2) was dissolved in 5 mL of ethanol and added to the nanoparticle solution. Normal nanoparticle NMR spectra show extreme peak broadening[1] but the iodine oxidizes the gold core and releases the ligands as disulfides. Disulfides exhibit almost identical peak shifts as the original thiol. The solution was then dried at 40 °C by rotary evaporation and re-dissolved in a minimum of dueterated chloroform. ^{1}H NMR spectra were acquired on a Varian 400 MHZ instrument. Spectral peaks corresponding to specific protons of the different ligands were integrated. The peak area was divided by the corresponding number of protons and the ratio of the two distinct peaks was taken as the ratio of the ligands. Figure A.1 shows the individual ligand peaks used and the corresponding proton spectrum. Figures A.2-A.4 show spectra corresponding to the nanoparticles prepared with 25%, 50%, and 75% MUA in solution are shown below. The red underlines represent the peaks used in determining the ligand ratio.

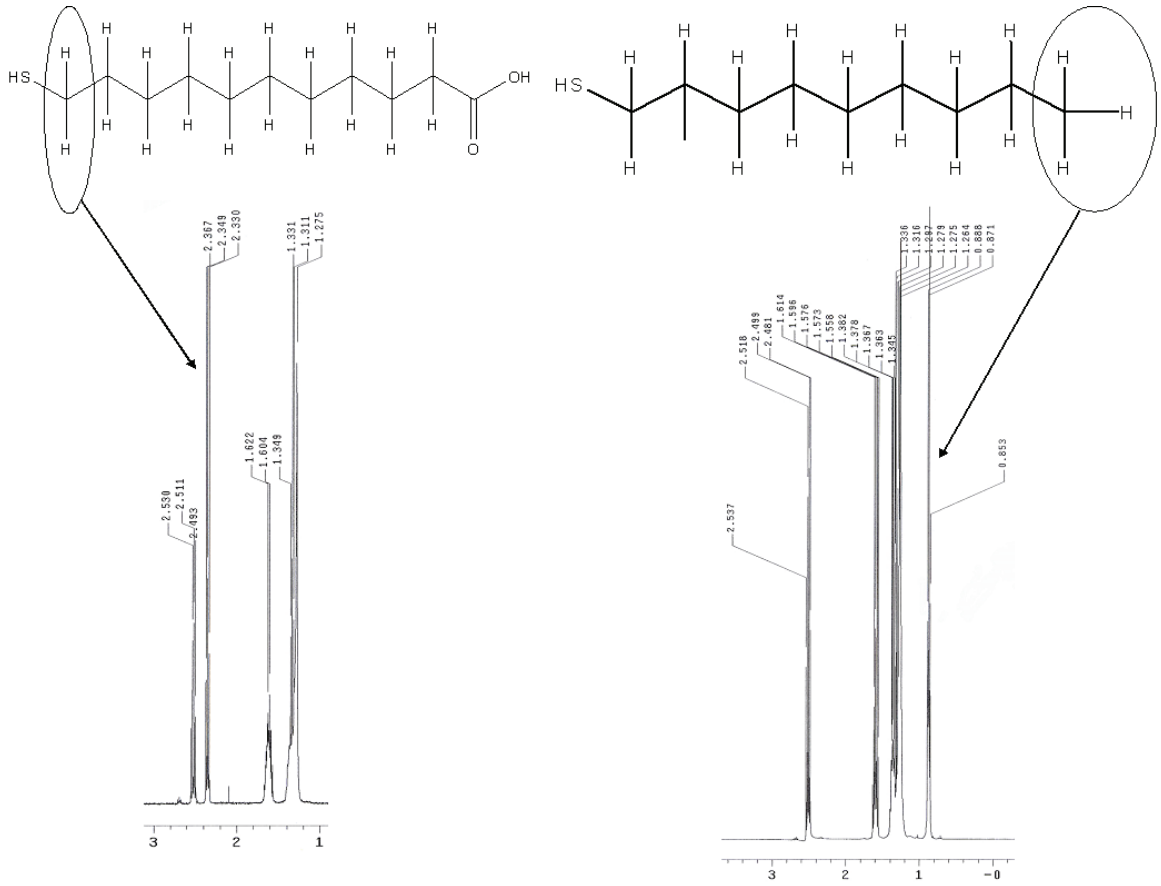

Figure A. 1: ^{1}H NMR spectra of pure thiol ligands in $CDCl_3$ with corresponding spectral peaks shown.

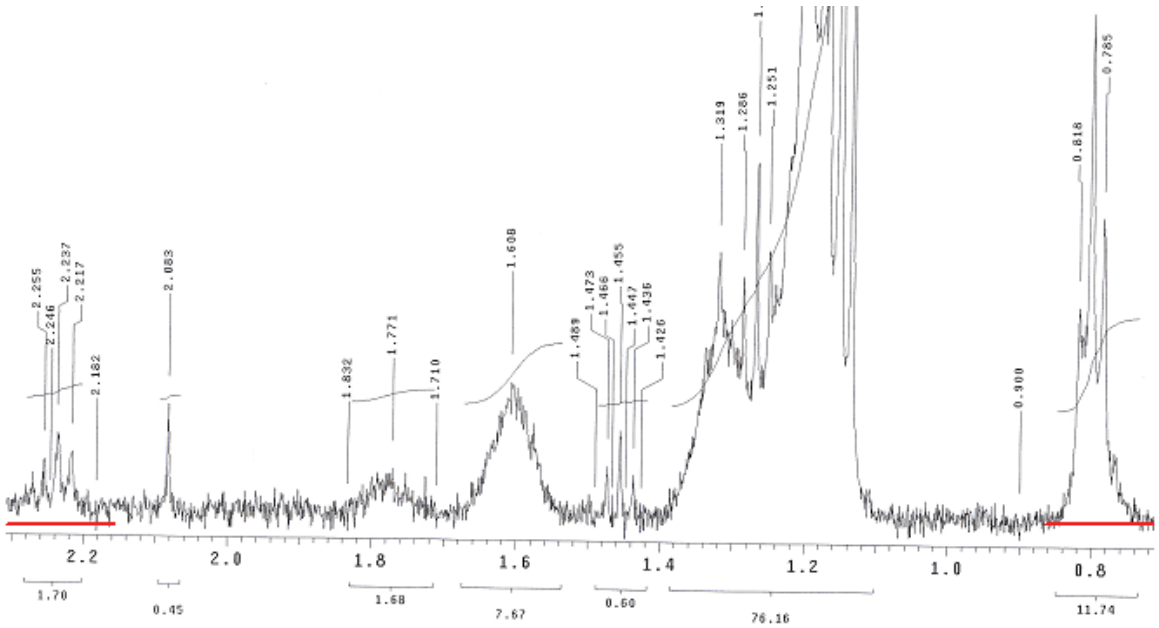

Figure A. 2: ^{1}H NMR spectrum of iodine-etched gold nanoparticles formed in a 25% MUA solution. Spectrum shows final MUA content is 18% on the gold nanoparticle surface.

Figure A. 3: ^{1}H NMR spectrum of gold nanoparticles prepared in a 50% MUA solution. Spectrum shows that the final nanoparticle MUA content is 37% on the nanoparticle surface.

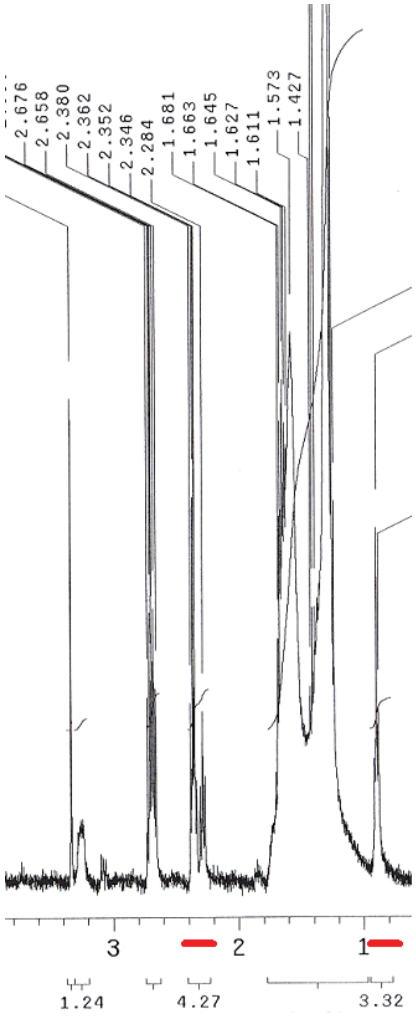

Figure A. 4: ^{1}H NMR spectrum of gold nanoparticles prepared in a 75% MUA solution. Spectrum shows that the final nanoparticle MUA content is 66% on the nanoparticle surface.

References

1. Wang, W.; Murray, R.W. *Langmuir*. **2005**, 21, 7015-7022.

2. Templeton, A. C.; Hostetler, M. J.; Kraft, C. T.; Murray, R. W. *J. Am. Chem. Soc.* **998**, *120*, 1906-1911.

CHAPTER 4

In Vitro Studies of Gold Nanoparticles in HeLa Cells

4.1 INTRODUCTION

Gold nanoparticle therapies have been developed for a range of biomedical agents *in vivo*. Cancer therapies such as tumor ablation[1] and delivery vehicles for anti-cancer drugs[2], MRI contrast agents[3], and gene delivery media[4] have all utilized nanoparticle scaffolds. Increased use of such applications of nanoparticles has resulted in a growing interest in the toxicological properties of nanoparticles. While much remains to be explored in relation to this problem, it has become clear that that targeted delivery can serve to minimize nanoparticle toxicology for *in vivo* applications. In this regard, the most commonly employed strategy relies on the use targeting peptides (Section 1.3.1). In addition to providing a means by which to target specific cell regions, targeting peptides can provide insight into the understanding of cell-nanoparticle interactions.

The design and *in vivo* localization of gold nanoparticles is the subject of this Chapter. Experiments involving the development of nuclear targeting fluorescent gold nanoparticles and the resulting cellular imaging are discussed. The imaging and cell cultures presented here were performed by Dr. An Beum-soo, a post-doctoral fellow in the lab of Dr. John White in the McGill University department of Physiology. The gold nanoparticle peptide conjugate protocol was developed by Dr. Andreas Peer, a post-doctoral fellow in the McGill University department of Chemistry. Tat-NLS conjugated FITC nanoparticles were in fact prepared by Dr. Andreas Peer.

.

4.2 MATERIALS

Peptide sequences were obtained from the Sheldon Biotechnology center at McGill University. Custom peptides were all functionalized with an N-terminal cysteine residue for the polyethylene glycol (PEG) conjugation. The peptide sequences are shown in Table 4.1. All cell work, performed by Dr. An Beum-soo, were carried out in HeLa cells cultivated in the facilities of the Department of Physiology. The functionalized PEG ligands used for the synthesis of the gold nanoparticles were synthesized by Dr. Andreas Peer.

Peptide Name (Short)	Peptide Sequence
Tat	CYGRKKRRQRRR
NLS	CGGFSTSLRARK

Table 4.1

4.3 METHODS

4.3.1 Gold Nanoparticle Preparation

The peptide gold nanoparticle conjugates were prepared using the DMAP exchange method described in Section 3.3.5. The thiol-DMAP exchange reaction was performed in aqueous solution containing 0.45×10^{-3} M total thiol with a thiol ratio 7:1:0.5 PEG_{45}-SH: FITC-PEG:Peptide-PEG. Purification was achieved using a Sephadex G-25 column eluted with MilliQ water.

4.3.2 Transmission Electron Microscopy (TEM)

All transmission electron microscopy (TEM) images were obtained using a Phillips CM200 microscope using 200 kV accelerating voltage. Samples were prepared by drop-casting an aqueous solution of gold nanoparticles on 200 mesh carbon coated copper grids (SPI Supplies, West Chester, PA).

4.3.3 Fluorescamine Assay

In order to test for the presence of peptide residues on the nanoparticle surfaces, the NLS functionalized gold nanoparticles were screened using a fluorescamine assay. Fluorescamine fluoresces when reacted with a primary amine and was thus chosen to test for the presence of peptides in the gold nanoparticle sample. The fluorescamine assay was carried out by first dissolving 30 mg of the fluorescamine reagent (Sigma-Aldrich Canada, Oakville, ON) in 100 mL of acetone. A peptide standard was prepared by dissolving 5 mg of NLS in 5 mL of PBS. 0.5, 2, 5, 10, 20, 30, 40, and 50 μL of this stock were then diluted in 1500 μL of PBS. 0.5 μL of the fluorescamine was added to each of these solutions and incubated for 5 minutes at room temperature before taking the fluorescence spectra. Spectra were obtained with a Cary Eclipse (Varian Inc., Walnut Creek, CA) using an excitation wavelength of 390 nm. The nanoparticle sample was then assayed by dissolving 1 mg of dry nanoparticle sample in 2 mL of PBS.

4.3.4 Cell Culture

Cell culture using HeLa cells was carried out in 1:1 mixture of Dulbecco's modified eagle medium containing 10% fetal bovine serum (FBS) at 37°C in 5% CO_2 atmosphere. The cells were then incubated with 10 uL of a 10 uM NP solution for 24 hrs. The cells were then centrifuged to remove nanoparticle containing medium and resuspended in culture medium for confocal imaging.

4.3.5 Confocal Microscopy

Confocal imaging was carried out using a Carl Zeiss LSM M510 microscope (Carl Zeiss AG, Germany) with an excitation wavelength of 488 nm and an emission

wavelength of >505 nm wavelength at 37°C. Microscope slides were counterstained with DAPI nuclear stain prior to imaging. Images were captured with XpressMicro software.

4.4 RESULTS

4.4.1 Nanoparticle Characterization

Fluorescent gold nanoparticle-peptide conjugates were characterized using TEM. The TEM images are shown in the layouts with the corresponding confocal micrographs.

4.4.2 Confocal Microscopy

Confocal microscopy images were obtained by separately exciting the nanoparticles and the nuclear dye. Cellular localization of the nanoparticles was determined by utilizing the fluorescence of the fluorescein isothiocyanate (FITC) ligand. An example of the standard control performed is provided in Figure 4.1, where the uptake of FITC-gold nanoparticles (no peptides) in HeLa cells is shown. FITC-gold nanoparticles are used to compare the efficiency of uptake and localization of the peptide labeled gold nanoparticles. The TEM inset (bottom right) shows the histogram of the nanoparticle size distribution. The size of the nanoparticles used was 5.1±1.2 nm.

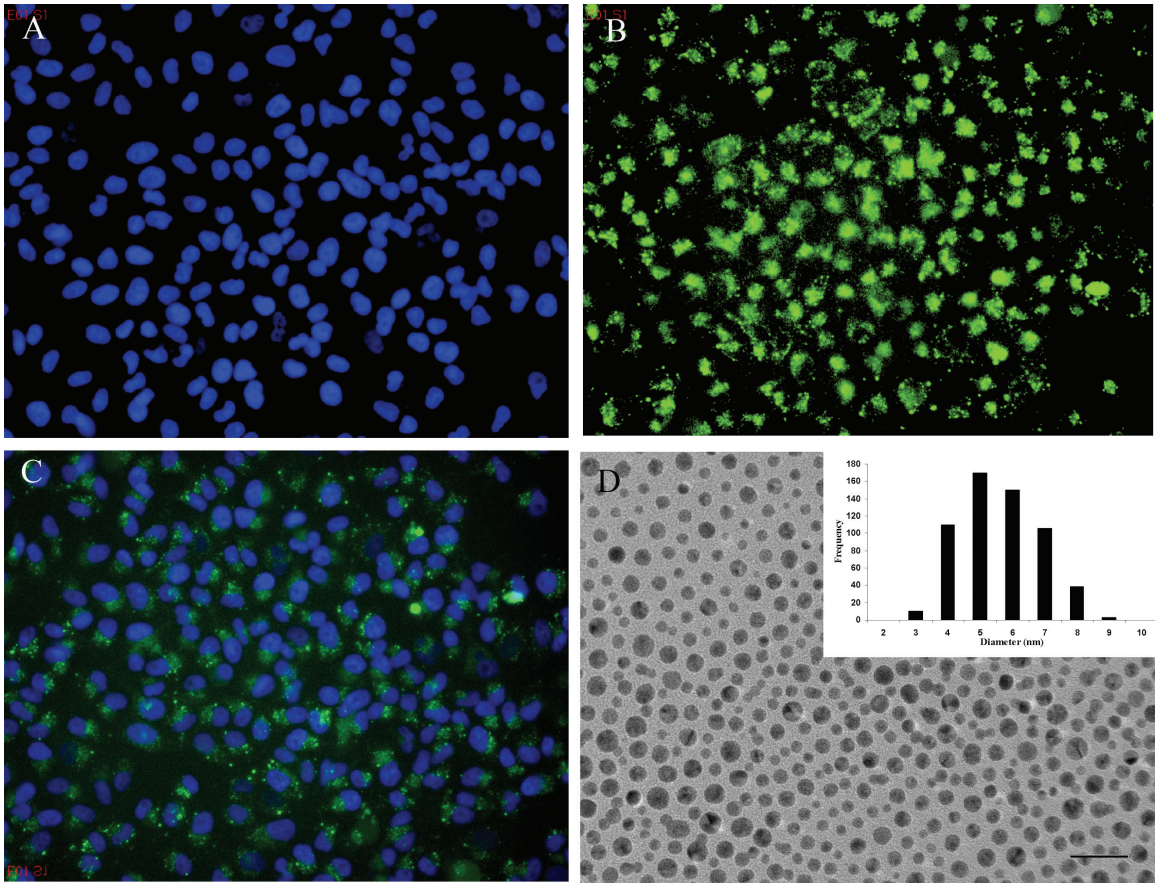

Figure 4.1: Cellular uptake of fluorescent (FITC) gold nanoparticles. The blue dye is a nuclear stain (top left). Green fluorescence is due to the gold nanoparticles (top right). An overlay of the nuclear and gold nanoparticle and nuclear fluorescence is shown on the bottom left. The bottom right is a TEM image of the FITC-gold nanoparticles used in the confocal experiments, the scale bar of the TEM image is 20 nm.

Gold nanoparticles labeled with both Tat, to facilitate uptake, and nuclear localization signal (NLS) (Section 1.3.1), were incubated with HeLa cells to examine the efficiency of uptake and nuclear localization of the targeting peptides. The TEM grids were prepared at dilute concentrations making statistical analysis of the core diameter impossible, although the TEM image shows similar sized nanoparticles, with respect to Figure 4.1. Figure 4.2 provides the confocal images of the cells incubated with nanoparticles as well as the TEM of the FITC-NLS-Tat-gold nanoparticles.

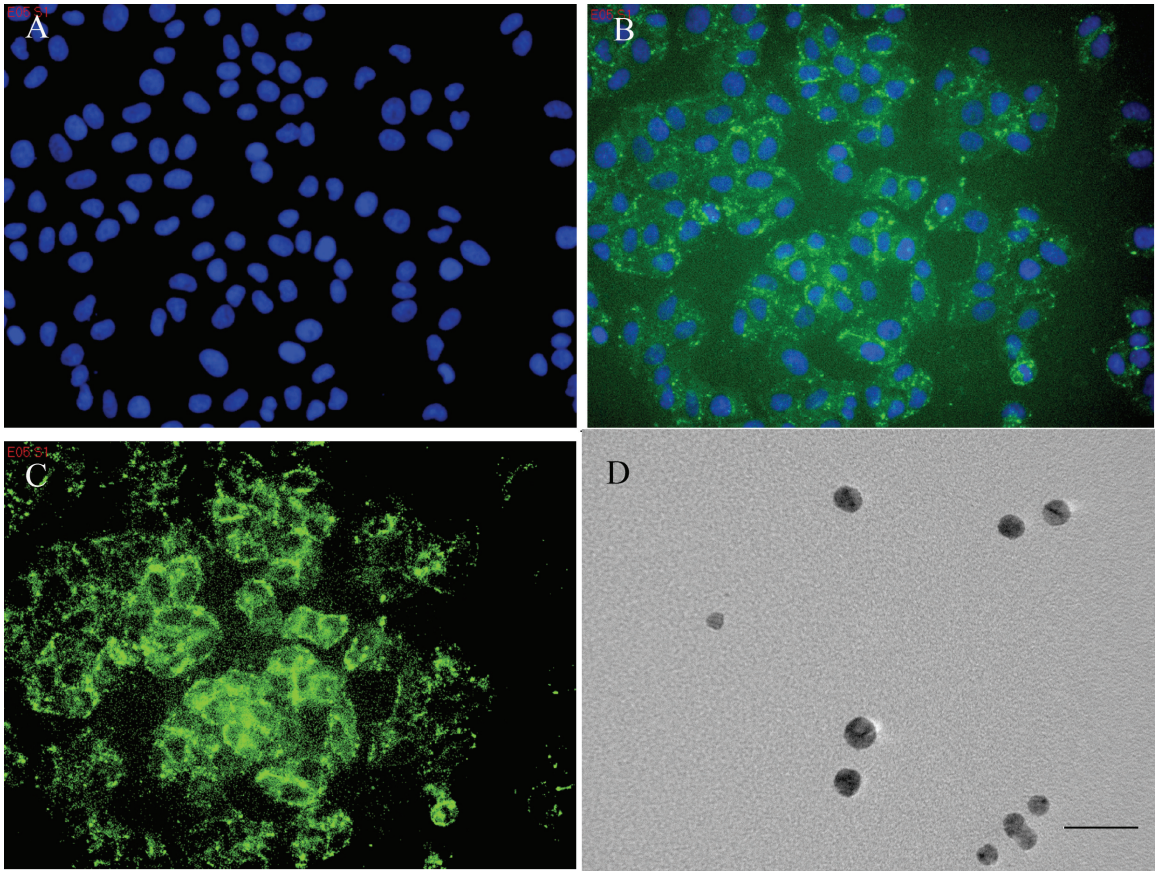

Figure 4. 2: Cellular uptake of fluorescent (FITC)-NLS-Tat-gold nanoparticles. The blue dye is a nuclear stain (A). Green fluorescence is due to the FITC-labeled gold nanoparticles (B). An overlay of the nuclear and gold nanoparticle and nuclear fluorescence is shown C. D is a TEM image of the FITC-NLS-Tat-gold nanoparticles used in the confocal experiments, the scale bar of the TEM image is 20 nm.

Finally, the HeLa cell uptake experiment was carried out using fluorescent gold nanoparticles with only an NLS targeting peptide. The best results overall were achieved using this formulation. The results are shown in Figure 4.3. As was the case with the NLS-Tat nanoparticles, TEM images did not contain sufficient nanoparticle density for an accurate statistical size analysis.

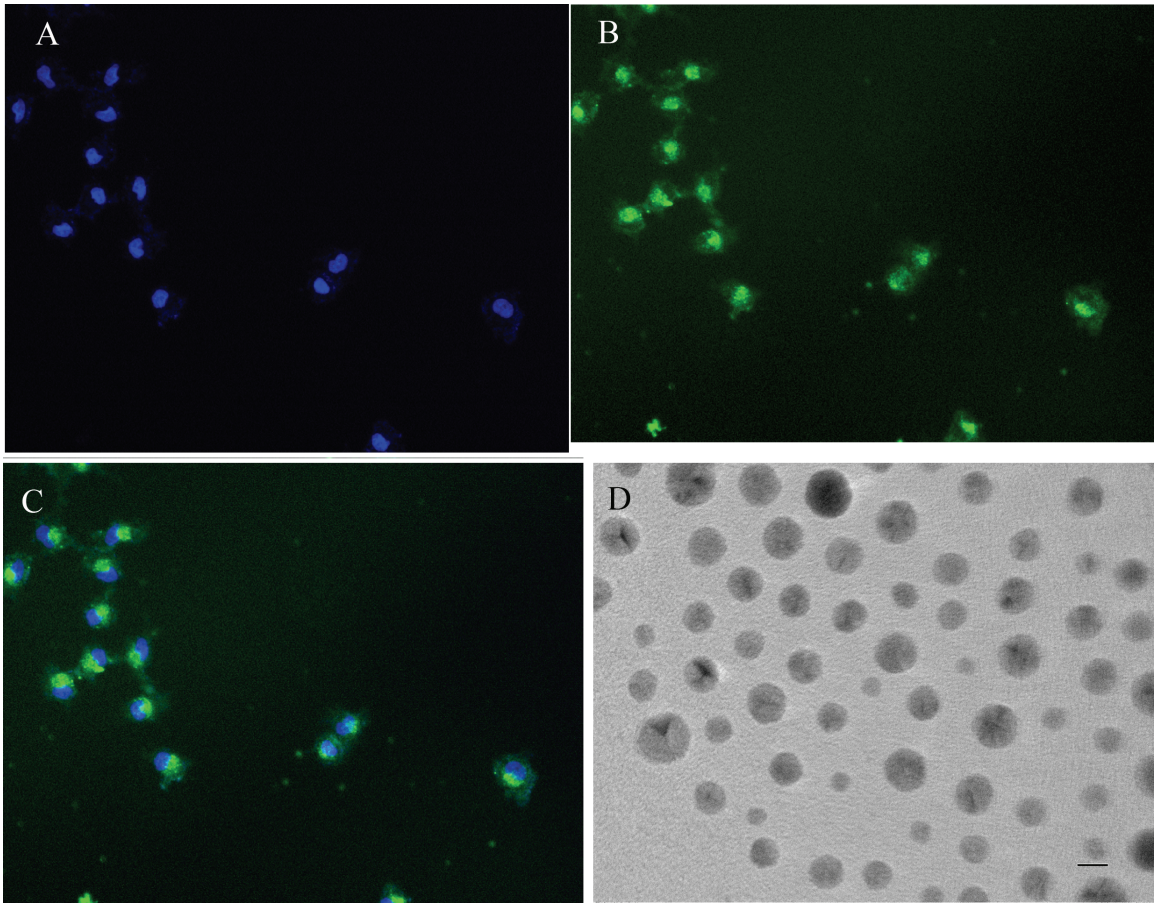

Figure 4. 3: Cellular uptake of fluorescent (FITC)-NLS-gold nanoparticles. The blue dye is a nuclear stain (A). Green fluorescence is due to the FITC-labeled gold nanoparticles (B). An overlay of the nuclear and gold nanoparticle and nuclear fluorescence is shown in C. D is a TEM image of the FITC-NLS-gold nanoparticles used in the confocal experiments, the scale bar of the TEM image is 5 nm.

4.5 DISCUSSION

Endosomal uptake (Section 1.3.1) is frequently encountered as the primary cellular uptake mechanism for nanoparticles[5-7]. Although uptake is the primary objective in such studies, endosomes hinder cellular localization by restricting nanoparticle movement into cellular organelles, including the nucleus. Nanoparticles taken up in endosomes frequently remain entrapped in these vesicles. For applications, as in the present study, such as nuclear targeting, endosomal entrapment is therefore highly undesirable. Figures 4.1 and 4.2, establish that endosomal entrapment of the

nanoparticles is clearly occuring. Endosomal nanoparticles can be discerned by the appearance of circular fluorescence patterns. The fact that minimal nanoparticle fluorescence is seen in the nuclei in Figures 4.1 and 4.2 may be the result of the widespread distribution of endosomal nanoparticles in these images. It is not surprising that the FITC gold nanoparticles (Figure 4.1) show no nuclear fluorescence, as the lack of targeting peptides makes crossing the nuclear pore complex unlikely. However the combination of peptides used in Figure 4.2 (Tat to facilitate uptake, and NLS for nuclear localization), should in principle readily reach the nucleus. Despite this promising targeting peptide combination, no significant nuclear-localized fluorescence is seen in the overlay of nanoparticle and nuclear fluorescence. The most successful nanoparticle tested was that containing solely a single targeting peptide ligand, NLS. The NLS-gold nanoparticles (Figure 4.3) exhibit the least endosomal uptake and significant nuclear fluorescence (overlay).

The results indicate that the Tat peptide, although useful for cellular uptake (the cells pictured in Figure 4.2 show more concentrated fluorescence than Figure 4.1), is not ideal for use as a targeting sequence with gold nanoparticles when combined with NLS. On the other hand, when used alone NLS shows efficient nuclear targeting. These results are rather surprising, as Tat-NLS has been shown to deliver antisense oligonucleotides to the nucleus[8]. An alternative explanation may be the nature of the uptake mechanism promoted by the Tat peptide (Section 1.3.1). As previously mentioned, Tat promotes endosomal uptake[9], which in this case may limit accumulation of particles outside the endosome. Although endosomal uptake cannot be discounted as an uptake mechanism in

the NLS-gold nanoparticle system (Figure 4.3), the images indicate that the nanoparticles are not retained in these vesicles.

References

1. El-Sayed, I. H.; Huang, X. H.; El-Sayed, M. A. *Cancer Lett.* **2006**, *239*, 129–135.

2. Paciotti, G. F.; Kingston, D. G. I.; Tamarkin, L. *Drug Development Research,* **2006**, 67, 47-54.

3. Jun, Y. W.; Huh, Y. M.; Choi, J. S.; Lee, J. H.; Song, H. T.; Kim, S. J.; Yoon, S.; Kim, K. S.; Shin, J. S.; Suh, J.-S. *J. Am. Chem. Soc.* **2005**, *127*, 5732–5733.

4. Patel, P. C.; Giljohann, D. A.; Seferos, D. S.; Mirkin, C. A. *Proc. Natl. Acad. Sci.* **2008**, 105. 17222-17226.

5. Verma, A.; Uzun, O.; Hu, Y.; Han, H. S.; Watson, N.; Chen, C.; Irvine, D.; Stellacci, F. *Nature Materials*, **2008**, 7, 589-595.

6. Liu, Y.; Franzen, S. *Bioconjugate Chem.* **2008**, *19* (5), 1009–1016.

7. Tkachenko, A. G.; Xie, H.; Coleman, D.; Glomm, W.; Ryan, J.; Anderson, M. F.; Franzen, S.; Feldheim, D. L. *J.Am.Chem.Soc*. **2003**, 125, 4700-4701.

8. Patel, P. C.; Giljohann, D. A.; Seferos, D. S.; Mirkin, C. A. *Proc. Natl. Acad. Sci.* **2008**, 105. 17222-17226.

9. Lindgren, M.; Hällbrink, M.; Prochiantz, A.; Langel, Ü. *Trends in Pharmacological Research*, **2000**, 21, 99-103.

CHAPTER 5

Conclusions and Future Work

1.1 CONCLUSIONS

The experiments performed describe the importance of the capping ligand in the interaction of gold nanoparticles with lipid bilayers. Though not surprising in itself, the results show a quantitative correlation between ligand structure and composition for the first time, as measured by a dye leakage assay. For gold nanoparticles containing varying ratios of octanethiol and 11-mercaptoundecanoic acid, it is shown that the leakage induced in the vesicle leakage assay is enhanced by increased octanethiol ratio. The vesicle assays confirm that gold nanoparticles can cross the cellular membrane in the absence of energetically assisted uptake. In an extension of the discussed interactions, it was found that PEG-ylated fluorescent gold nanoparticles are most efficiently taken up into cells when labeled with a single targeting peptide, NLS, as opposed to using a combination of peptides.

1.2 FUTURE WORK

Because of the extent of *in vivo* use of gold nanoparticles today, the work described can have far reaching implications. The most logical continuation of this project would be to test the gold nanoparticles used in the leakage assay in an *in vitro* cell assay and correlate the findings in a cell model. New nanoparticle formulations need to be explored using the leakage assay developed. In order to compare the charge of the ligands to the type and extent of interaction the mercaptoundecanoic acid should be replaced by a cationic, hydrophilic ligand, such as an ammonium terminal thiol. The

hydrophobic to hydrophilic ligand ratio could once more easily be varied using the DMAP exchange method. Yet again, the leakage assay for these new particles should be examined in an *in vitro* cell assay. *In vitro* assays of this sort could be used to distinguish between passive and active transport by changing the temperature of the cell cultures. At 37°C both active and passive transport mechanisms are available, but at 4 °C only passive transport mechanisms are available. Conclusive data from the above mentioned experiments has the potential to yield a comprehensive understanding of the factors influencing the interaction of ligand-capped gold nanoparticle with lipid bilayers and cell membranes that has not been achieved today.